Sun-to-Earth Modeling of Coronal Mass Ejections with a Global MHD Model: Facilitating Physical Understanding and Space Weather Forecasting

Meng Jin

[1]Lockheed Martin Solar and Astrophysics Lab (LMSAL), Palo Alto, CA, USA
[2]SETI Institute, Mountain View, CA 94043, USA

Collaborators:

University of Michigan: Manchester, W. B., van der Holst, B., Sokolov, I. V., Toth, G., Borovikov, D., Welling, D., Gombosi, T. I.
LMSAL: Schrijver, C. J., Cheung, M. C. M., Nitta, N. V., Liu, W., DeRosa, M. L., Title, A. M.
Stanford University: Petrosian, V., Omodei, N., Rubio da Costa, F., Allafort, A.
NASA GSFC: Mullinix, R. E., Taktakishvili, A., Chulaki, A., Ofman, L.
Meng, X. (NASA/JPL), de Koning, C. A. (University of Colorado), Effenberger, F. (Helmholtz Centre Potsdam, Germany), Li, G. (University of Alabama), Pesce-Rollins, M. (Istituto Nazionale di Fisica Nucleare, Italy), Downs, C. (Predictive Science Inc.)

ISEST 2018 Workshop
September 24-28, 2018, Hvar, Croatia

Outline

- Coronal Mass Ejections (CMEs) are one of the major sources of destructive space weather. Our understanding of CMEs and their interplanetary propagation has been greatly improved over the last 46 years (*e.g., LRSP by Webb & Howard, 2012; a recent review book by Zhang+2018 based on ISEST project*).

- However, insufficient observation is still a limitation factor for deepening our theoretical understanding of CMEs. First-principles-based numerical models (e.g., *Usmanov & Dryer 1995, Wu+1999, Odstrcil+1999, Manchester+2004, Lugaz+2007, Toth+2007, Cohen+2008, Feng+2010, Shen+2011, Zhou+2012, Lionello+2013, van der Holst+2014, Pinto+2017, Scolini+2017, Torok+2018*) play a vital role in interpreting observations, testing theories, and providing forecasts.

- In this talk, we present the results based on several realistic CME events to demonstrate how the unique information provided by the MHD model could facilitate our understanding of fundamental processes of solar and heliophysics.

- We will also discuss how to transfer a research model for operational space weather forecast by determining model parameters from available near-Sun observations.

Alfvén Wave Solar Model (AWSoM)

$$\frac{\partial \rho}{\partial t} + \nabla \cdot (\rho \mathbf{u}) = 0 \quad (1)$$

$$\frac{\partial(\rho \mathbf{u})}{\partial t} + \nabla \cdot \left(\rho \mathbf{u}\mathbf{u} - \frac{\mathbf{B}\mathbf{B}}{4\pi}\right) + \nabla\left(p_p + p_e + \frac{w_+ + w_-}{2} + \frac{B^2}{8\pi}\right) = -\rho \frac{G M_\odot}{r^2} \mathbf{e}_r \quad (2)$$

$$\frac{\partial \left(\frac{p_e}{\gamma - 1}\right)}{\partial t} + \nabla \cdot \left(\frac{p_e}{\gamma - 1}\mathbf{u}\right) = -p_e \nabla \cdot \mathbf{u} + \frac{2}{\tau_{pe}}(p_p - p_e) - \nabla \cdot \mathbf{q}_e - Q_{rad} + \alpha Q_w \quad (3)$$

$$\frac{\partial \left(\frac{p_p}{\gamma - 1}\right)}{\partial t} + \nabla \cdot \left(\frac{p_p}{\gamma - 1}\mathbf{u}\right) = -p_p \nabla \cdot \mathbf{u} + \frac{2}{\tau_{pe}}(p_e - p_p) + (1 - \alpha) Q_w \quad (4)$$

$$\frac{\partial w_\pm}{\partial t} + \nabla \cdot [w_\pm(\mathbf{u} \pm \mathbf{u}_A)] = -\frac{w_\pm}{2} \nabla \cdot \mathbf{u} - \Gamma_\pm w_\pm \quad (5)$$

$$\frac{\partial \mathbf{B}}{\partial t} - \nabla \times (\mathbf{u} \times \mathbf{B}) = 0 \quad (6)$$

- Developed within Space Weather Modeling Framework (SWMF; Toth et al. 2005, 2012) at University of Michigan.
- Coronal heating and solar wind accelerating by Alfven waves. Physically consistent treatment of wave reflection, dissipation, and heat partitioning between the electrons and protons.
- Model starts from upper chromosphere including heat conduction (both collisional and collisionless) and radiative cooling.
- Adaptive mesh refinement (AMR) to resolve structures (e.g., current sheets, shocks).
- Data-driven inner boundary condition by synoptic magnetograms (e.g., GONG, MDI, HMI).

References: van der Holst et al. 2010, Manchester et al. 2012, Jin et al. 2012, Sokolov et al. 2013, Oran et al. 2013, Jin et al. 2013, van der Holst et al. 2014

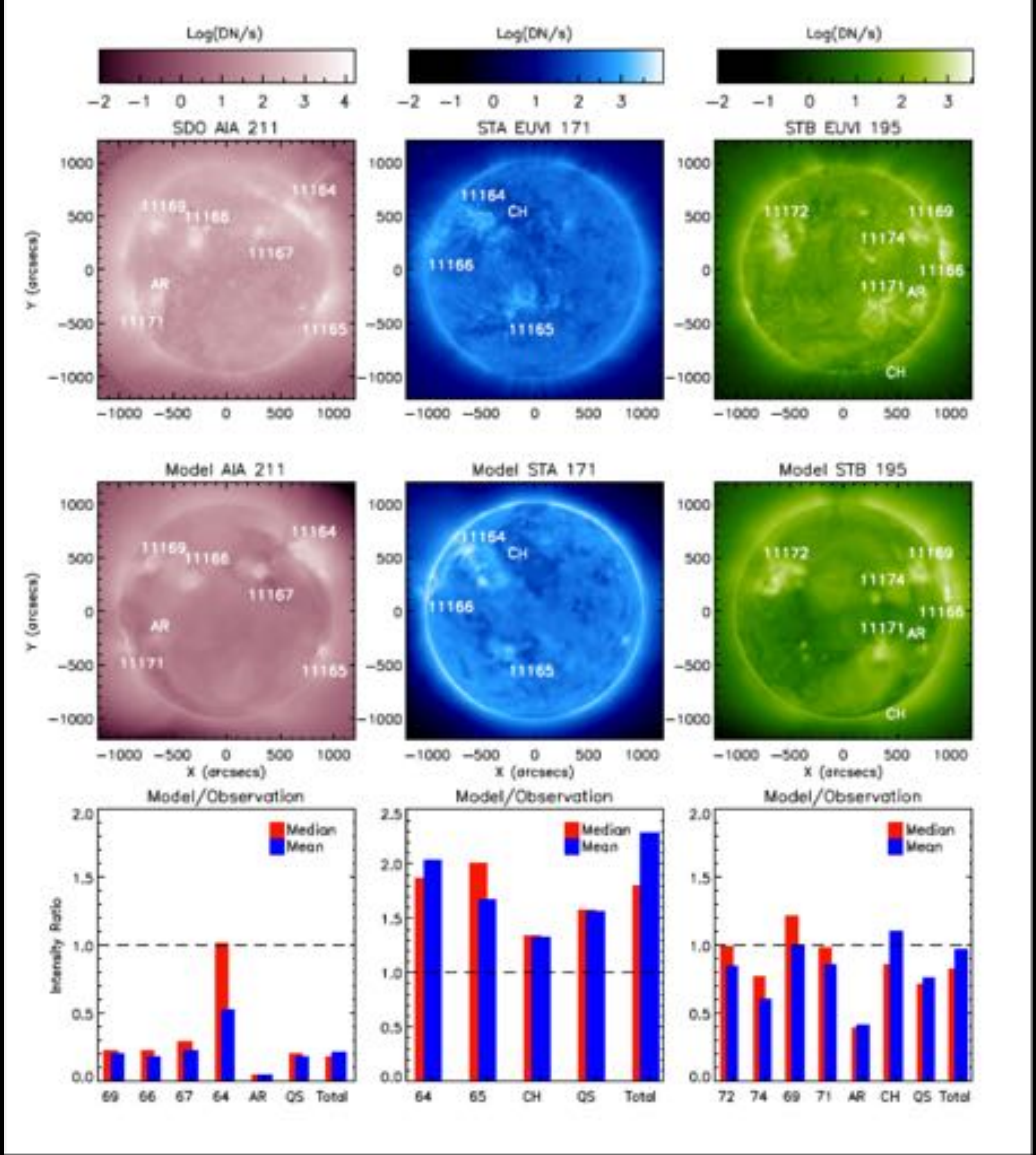

The Comparison between Observations and Synthesized EUV Images of the Steady State Solar Wind Model

Top panels:
Observational images from SDO AIA 211, STEREO A EUVI 171, and STEREO B EUVI 195. The observation time: **2011 March 7 ~20:00 UT.**

Middle panels:
Synthesized EUV images of the model.

Bottom panels:
Quantitative comparison between the model and observation for different structures of the Sun.

Jin et al. 2017a

Gibson-Low Flux Rope

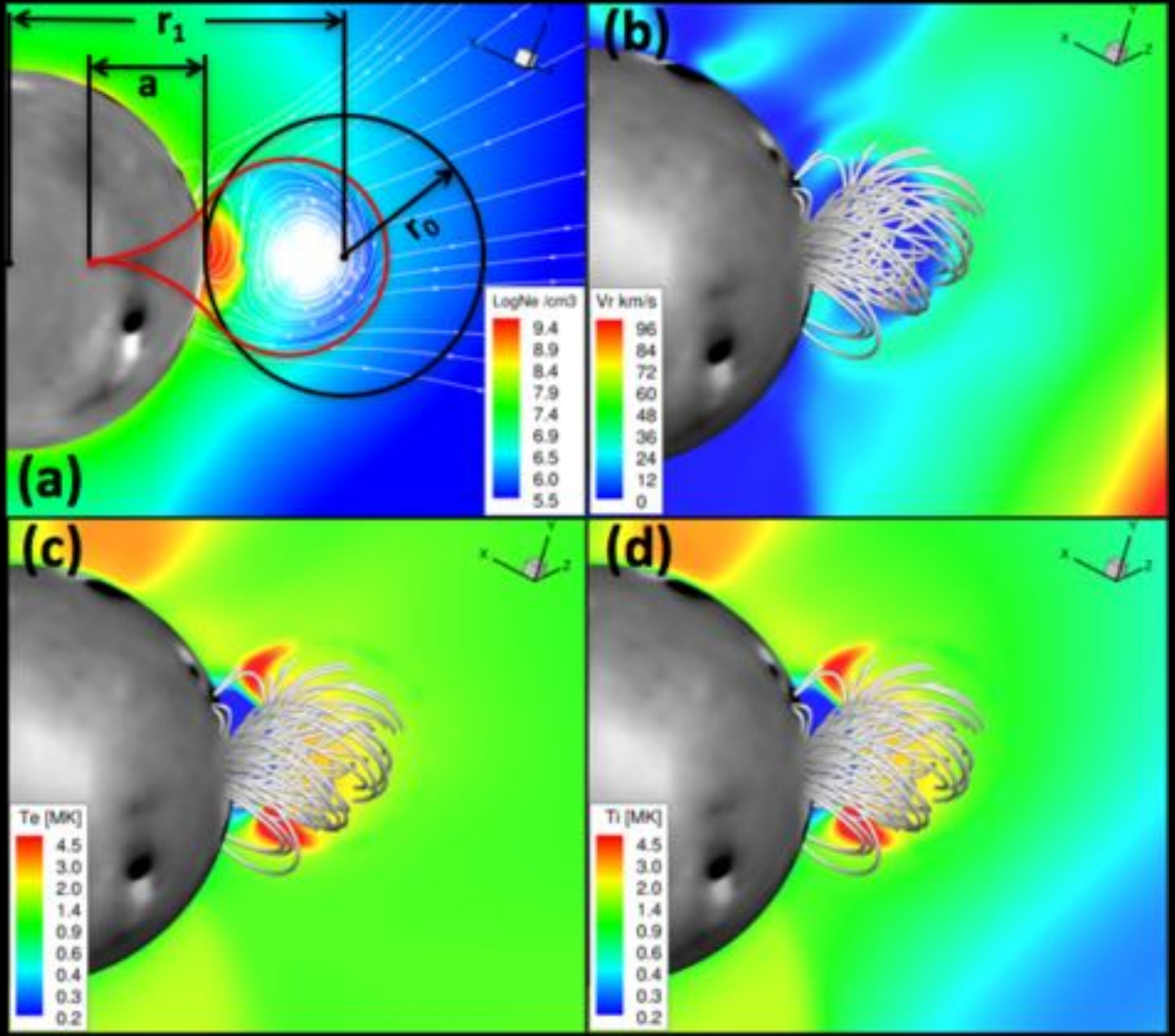

- Analytical profiles of the GL flux rope are obtained by finding a solution to the magnetohydrostatic equation and the solenoidal condition (*Gibson & Low 1998*) through mathematical stretching transformation.

- The transformed flux rope appears as a tear-drop shape of twisted magnetic flux.

- Lorentz forces are introduced, which leads to a density-depleted cavity in the upper portion and a dense core at the lower portion of the flux rope (3-part CME density structure).

The GL Flux Rope is determined by 5 parameters:

- a: determines the shape of the flux rope
- r_1: determines the initial position of the flux rope before it is stretched
- r_0: determines the size of the flux rope
- a_1: determines the magnetic strength of the flux rope
- Helicity Parameter: determines the positive (dextral)/negative (sinistral) helicity

CME Events

- In this talk, we will present four realistic CME events simulation, following each event, we focus on different physical processes during the CME evolution from the Sun to 1 AU.
- Event I: 2017 September 10 (New Campaign Event)
  - Global EUV waves [Impulsive Phase]
- Event II: 2011 February 15
  - Coronal Dimming [Impulsive Phase, Residual Phase]
- Event III: 2014 September 1 (Fermi Behind-the-limb Event)
  - CME-driven shocks, Gamma-ray emission [Impulsive Phase]
- Event IV: 2011 March 7
  - Shock connectivity and in-situ SEP, CME propagation in the heliosphere [Residual Phase, Propagation Phase]

2017 September 10 X8.2 Event

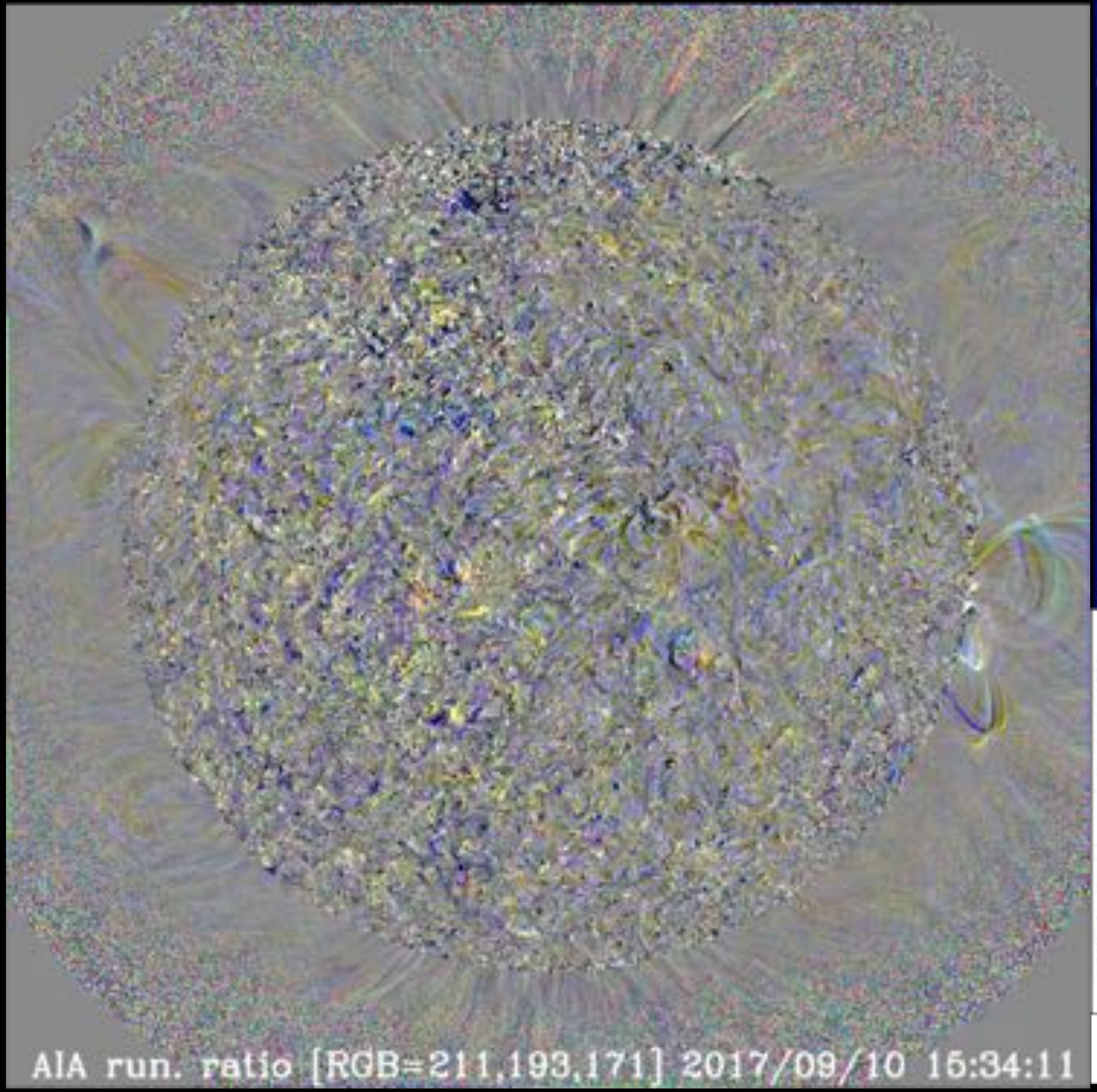

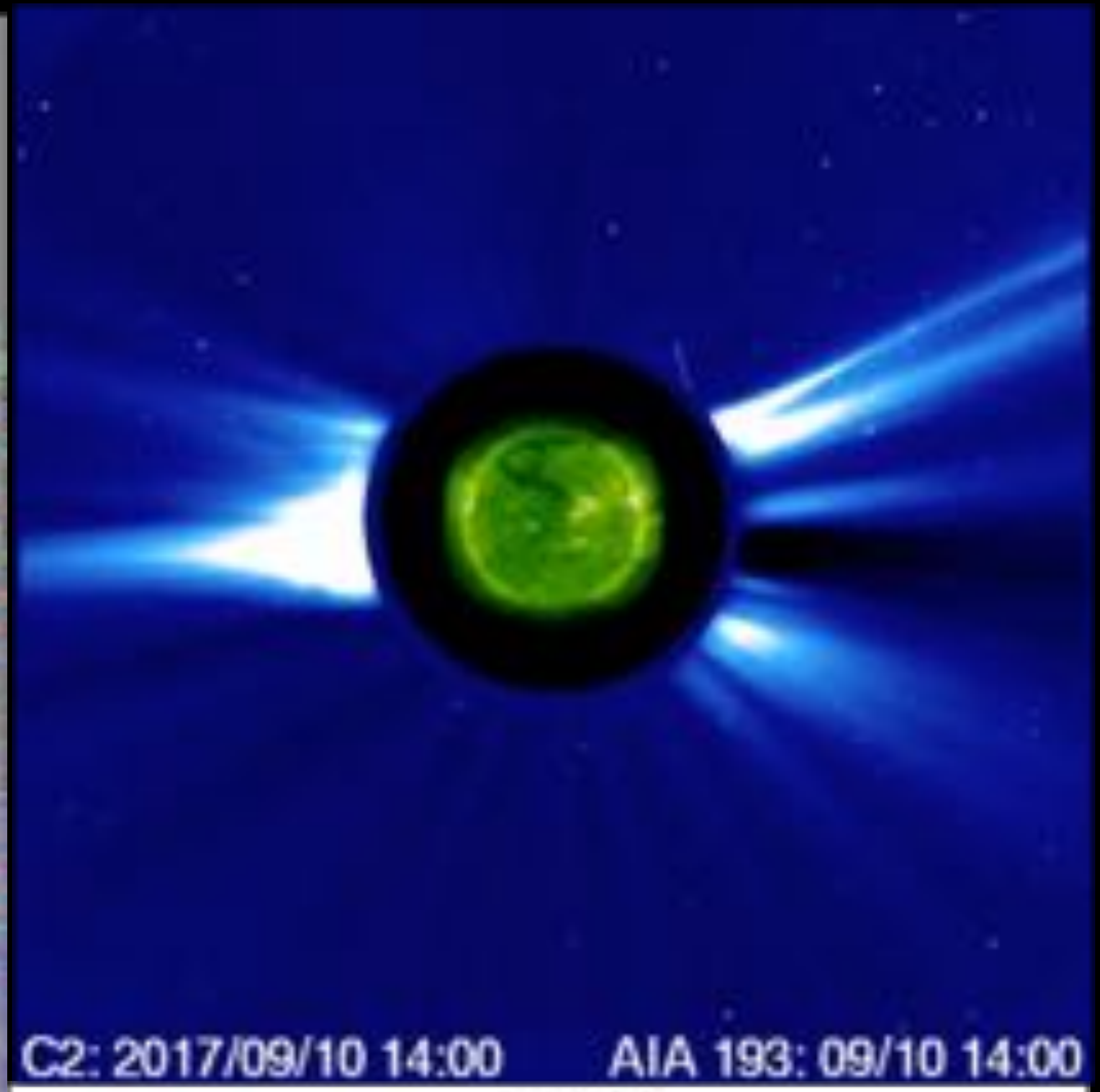

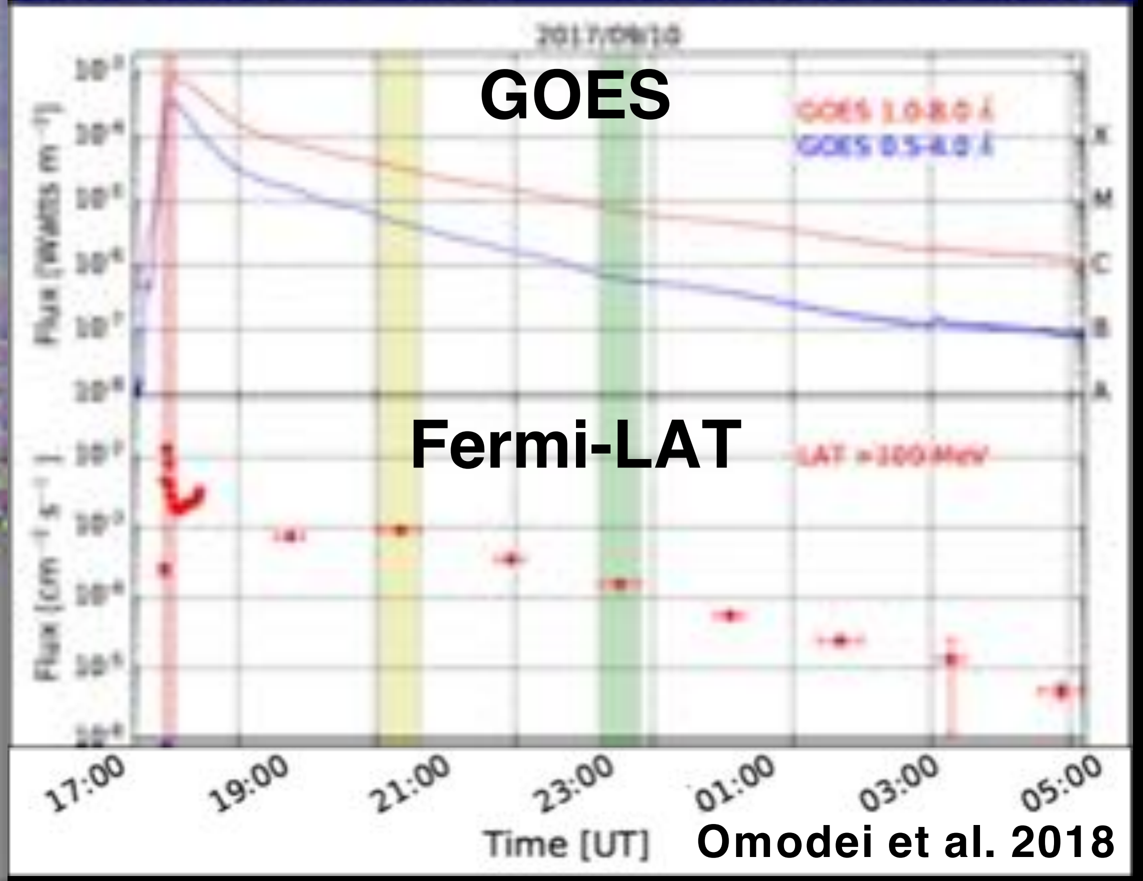

10-Sep-2017 X-flare ADS list by Peter Young: https://bit.ly/2Kbzlvb

- 2017 September 10 X8.2 flare event is associated with spectacular global EUV waves that transverse the entire visible solar disk (*Veronig et al. 2018, Liu et al. 2018*).
- A CME with speed > 3000 km/s, which is one of the fastest CMEs ever recorded.
- Solar Energetic Particles (SEPs) and Ground Level Enhancement (GLE) events at Earth.
- *Fermi-LAT* observed long-duration gamma-ray emission over 12 hours (Omodei et al. 2018).

Gibson-Low Flux Rope Setting

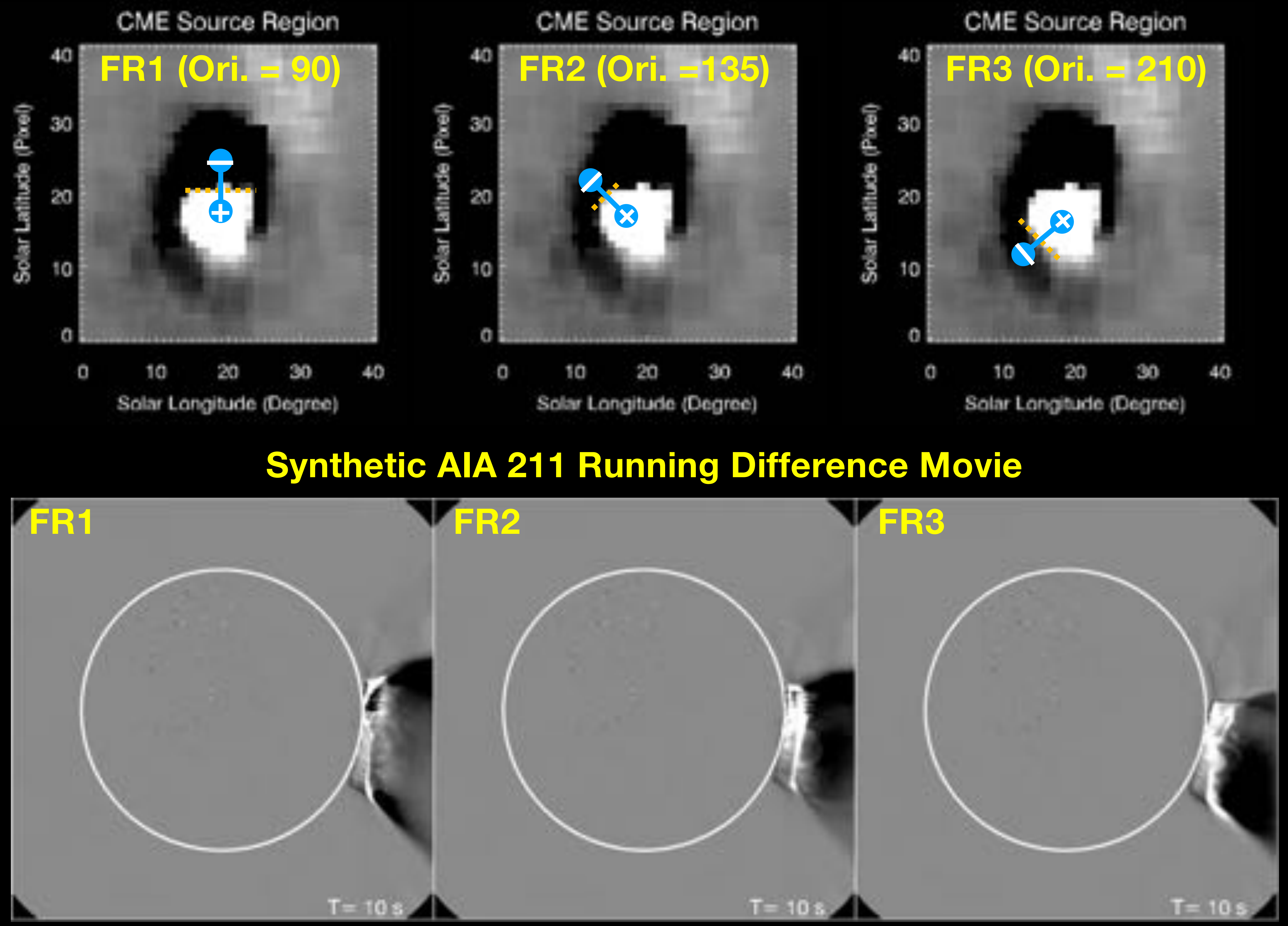

- 2017 September 10 event occurred at the **west limb**. Without direct observation of the source region, it is uncertain which **PIL** the eruption was initiated.
- Based on the magnetic field configuration of the source region, we initiate CMEs from three **PILs** with different flux rope orientations.
- **The resulting EUV waves show different features.**

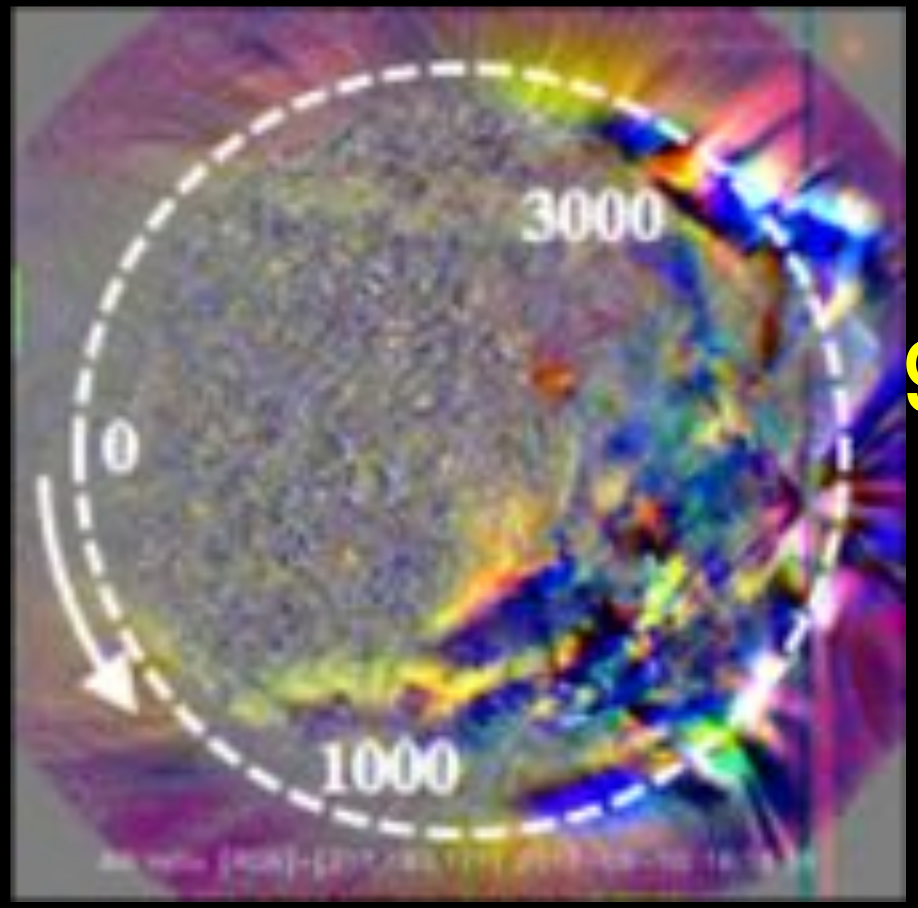

Time-slice from the Over-limb Azimuthal Cuts

Distance measured from origin in CCW direction, then mapped down to the limb.

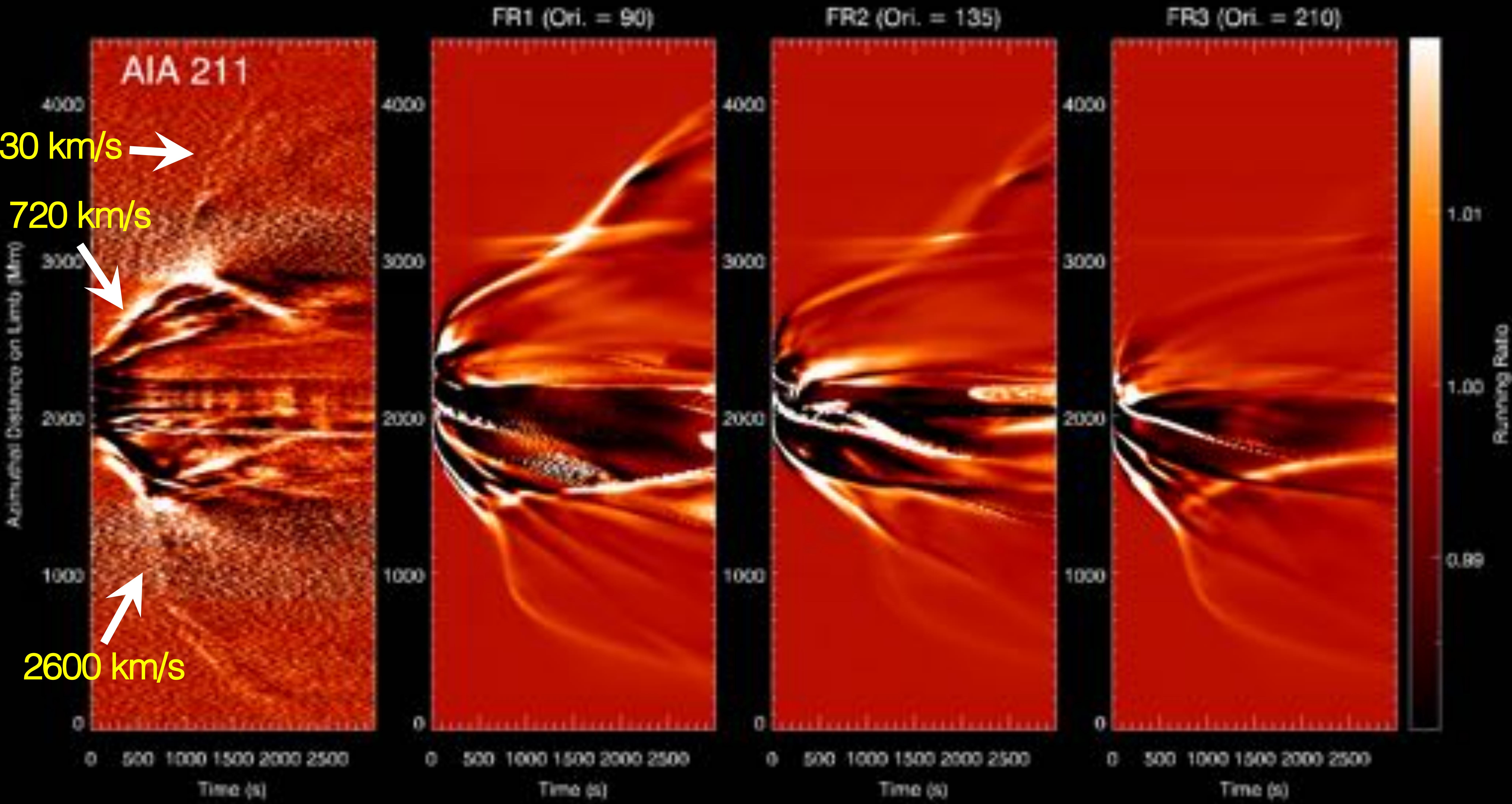

- With different flux rope orientations, the EUV waves show different features among three cases.
- In general, the flux rope with 90 degree orientation reproduces observation better the other two cases.

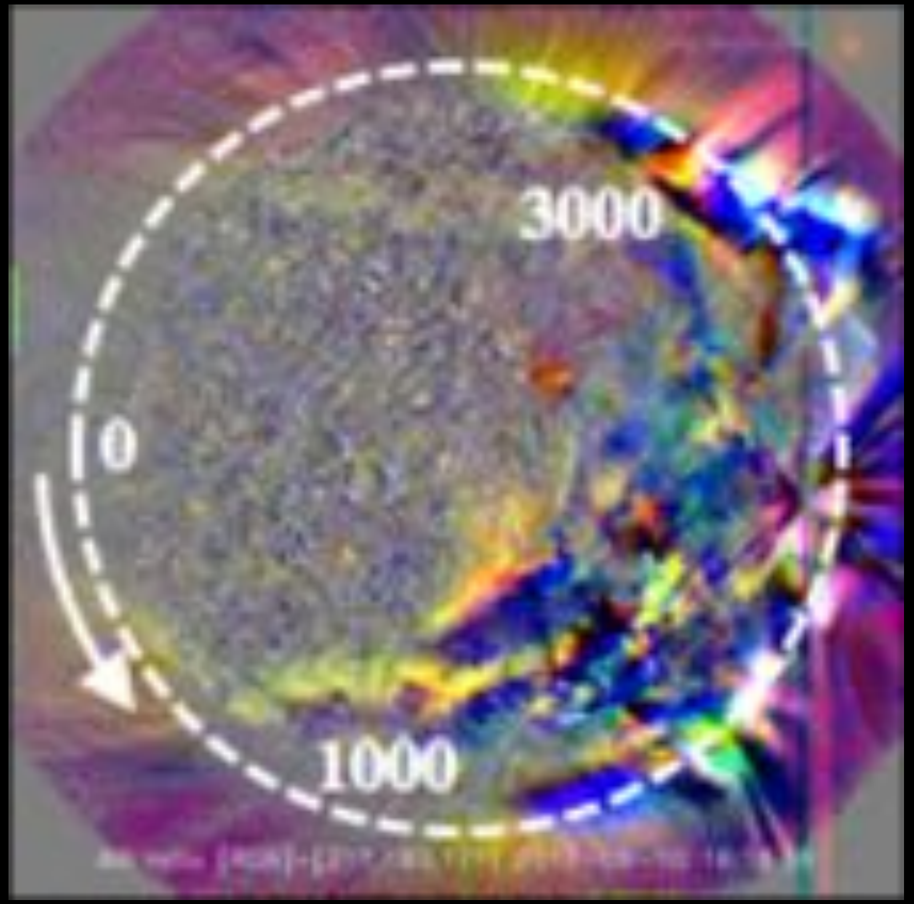

Time-slice from the Over-limb Azimuthal Cuts

Distance measured from origin in CCW direction, then mapped down to the limb.

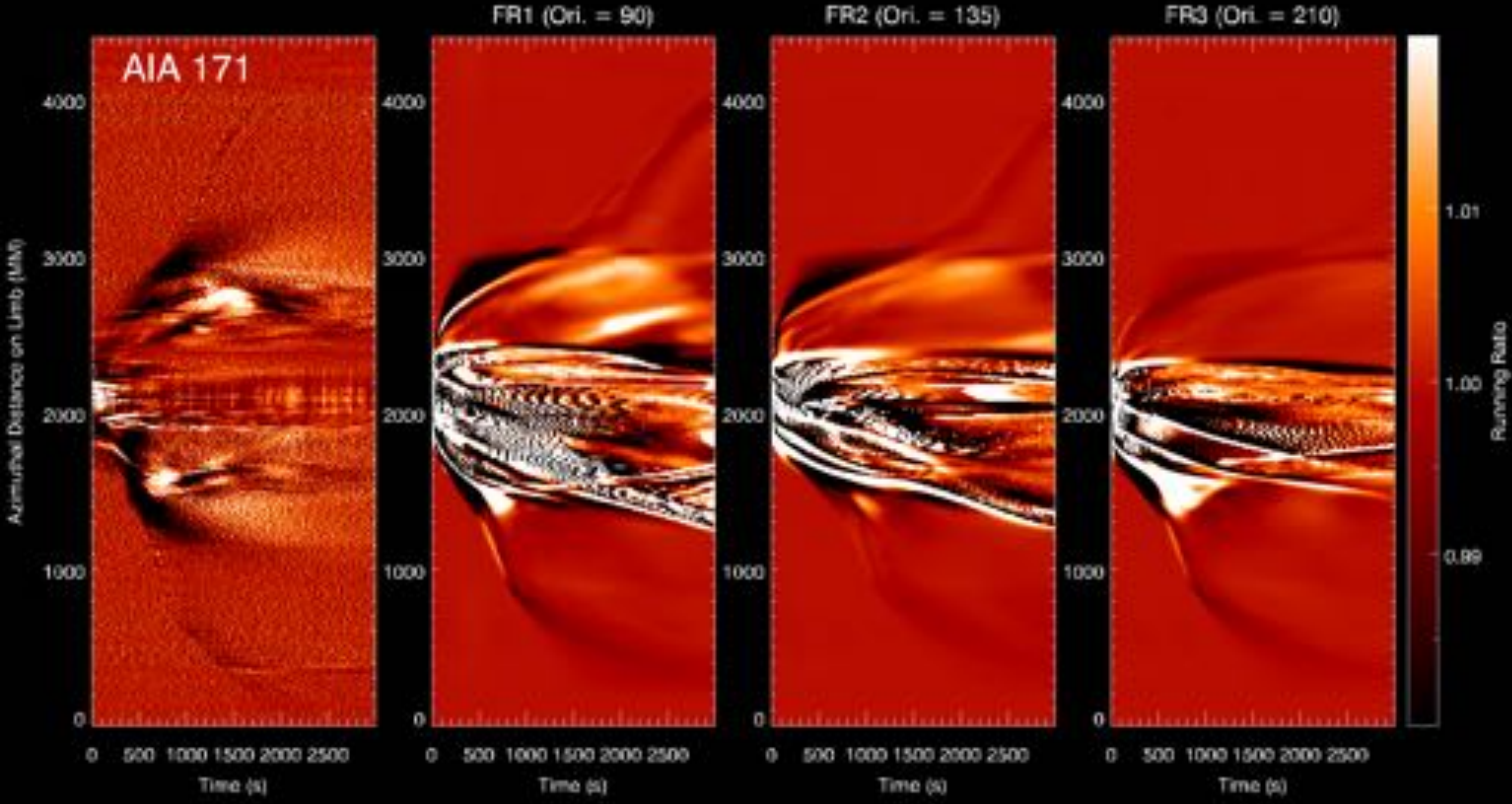

- The waves show darkening in 171 and brightening in 211, which suggest heating of the local plasma.
- **The EUV waves observation from AIA allows us to constrain the erupting magnetic configuration.**

Coronal Dimming

- Coronal dimming is the reduction in intensity on/near the solar disk across a large area, which has been observed in many wavebands (e.g., white-light, X-ray, EUV) of solar observation. And it is usually associated with coronal EUV waves.
- Spectroscopic observations confirmed that the dimmings are regions of up-flowing expanding plasma (e.g., *Harra & Sterling, 2001, Harra et al. 2007, Imada et al. 2007, Jin et al. 2009, Attril et al. 2010, Tian et al. 2012*). Both observation and MHD Modeling of solar coronal dimming (e.g., *Cohen et al. 2009, Downs et al. 2012*) suggest that the coronal dimming is mainly caused by the CME-induced plasma evacuation, and the spatial location is well correlated the footpoints of the erupting magnetic flux system (*Downs et al. 2015*).
- Solar observations suggest that all coronal dimmings were associated with CMEs. Therefore, they might encode important information about CME’s mass, speed, energy etc. (e.g., *Hudson et al. 1996, Sterling & Hudson 1997, Harrison et al. 2003, Zhukov & Auchere 2004, Aschwanden et al. 2009, Cheng & Qiu 2016, Krista & Reinard 2017, Dissauer et al. 2018*).
- *Harra et al. (2016)* found “coronal dimming is the only signature that could differentiate powerful flares that have CMEs from those that do not”. Therefore, dimming might be one of the best candidates to observe the CMEs on distant Sun-like stars.

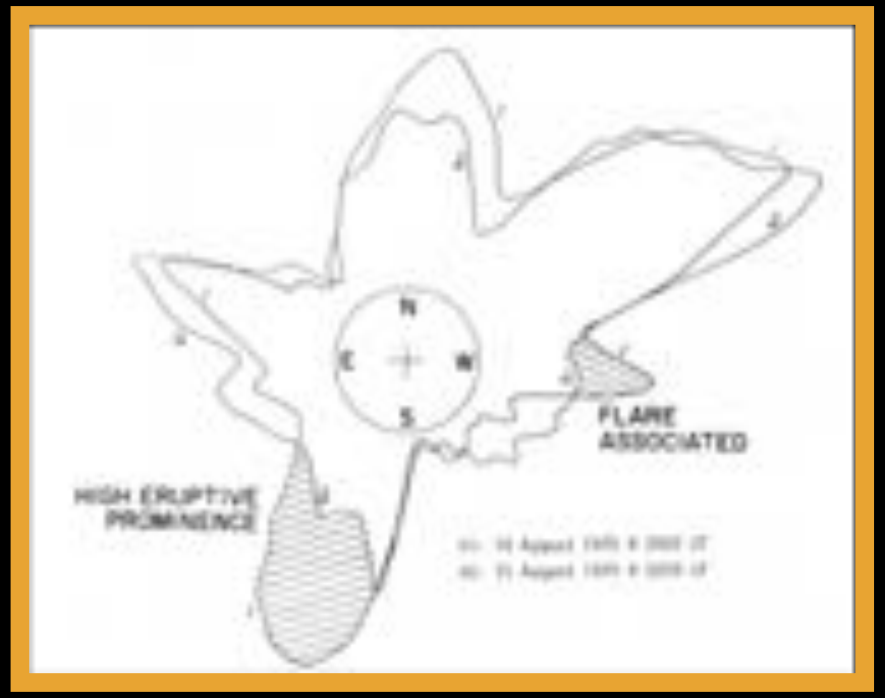

White-light corona “depletion” (Hansen et al. 1974)

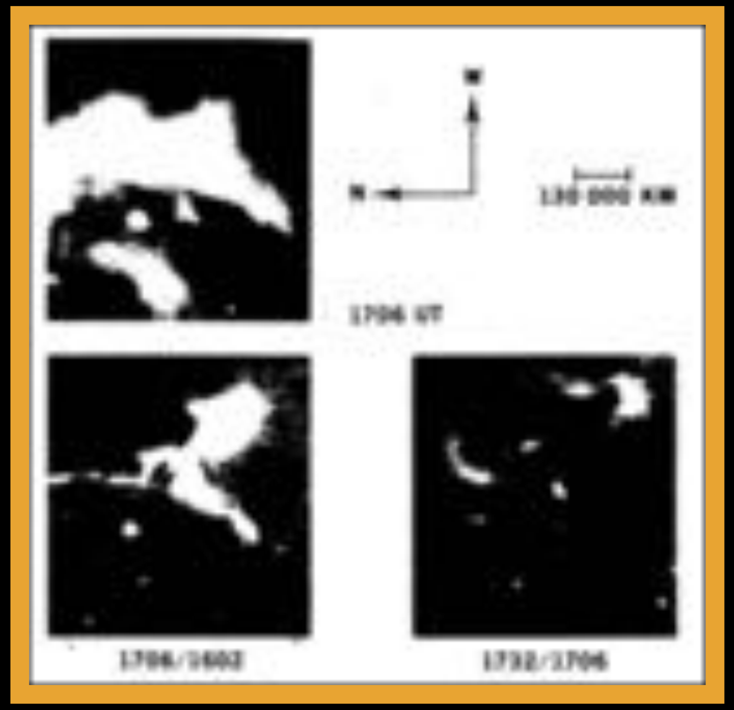

X-ray “transient coronal holes” (Rust and Hildner, 1976)

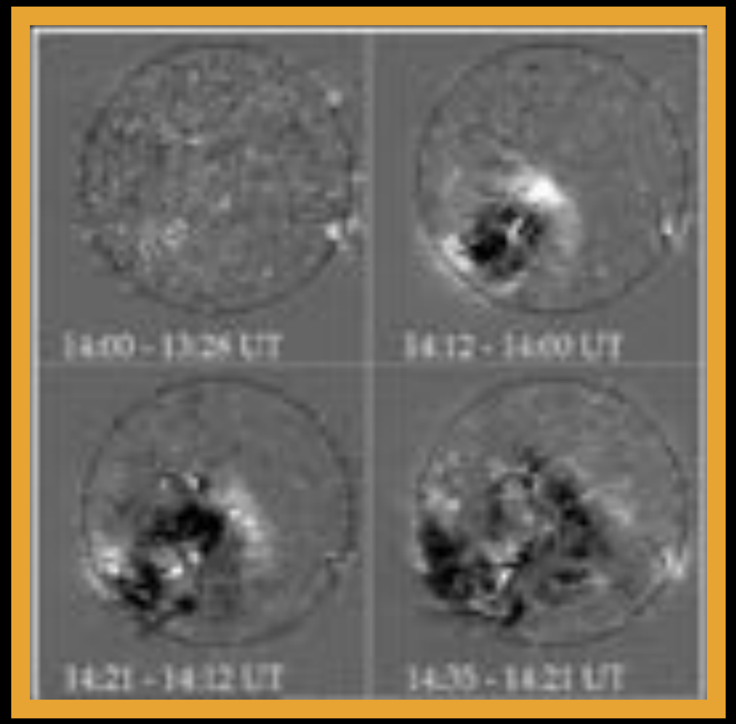

EUV Dimming by SOHO/EIT (Thompson et al. 1999)

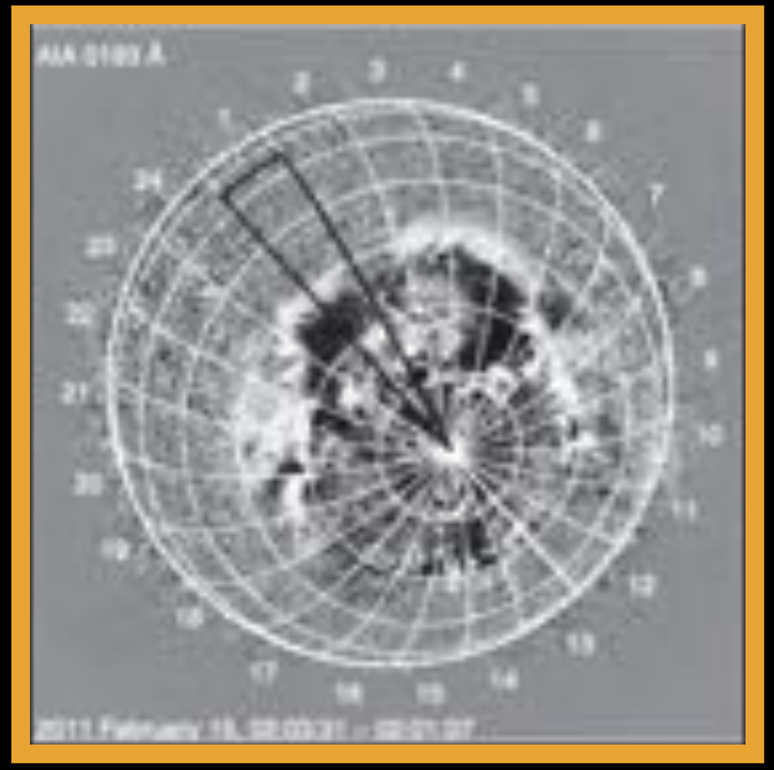

EUV Dimming by SDO/AIA (Nitta et al. 2013)

Observed Coronal Dimming/Brightening

AIA 171 (T = 0.63 MK)

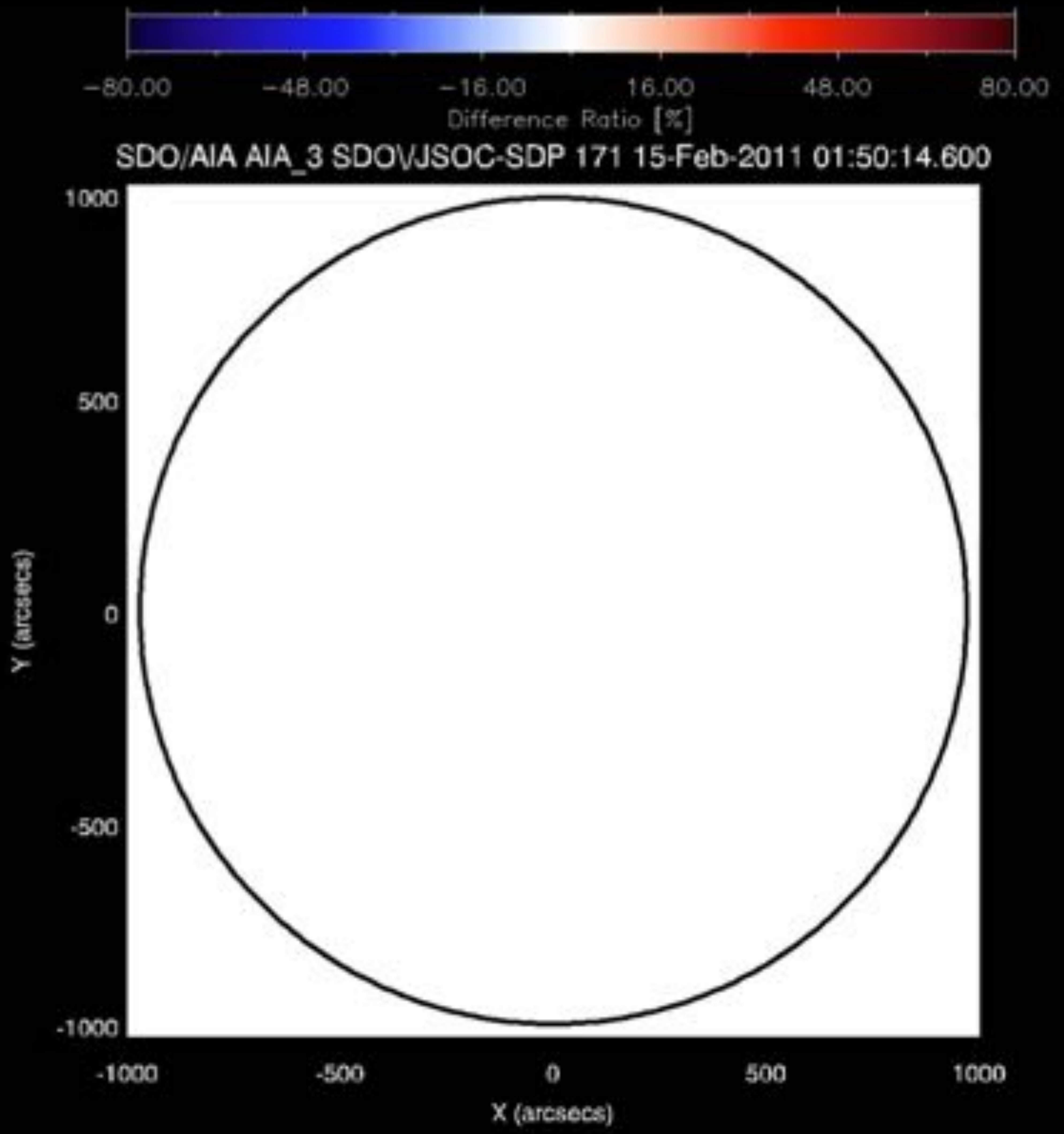

AIA 211 (T = 1.86 MK)

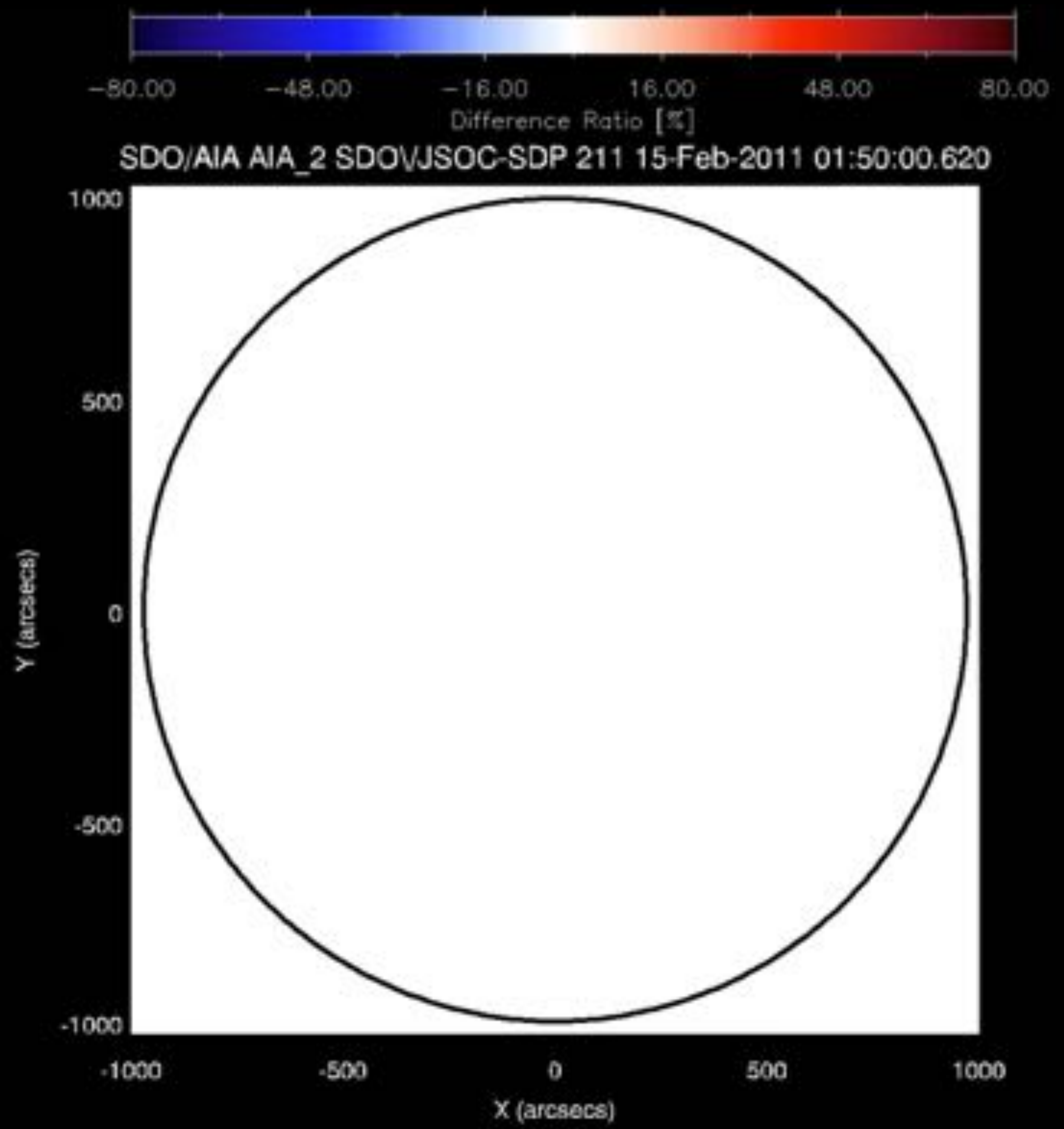

Synthesized Coronal Dimming/Brightening

AIA 171 (T = 0.63 MK)

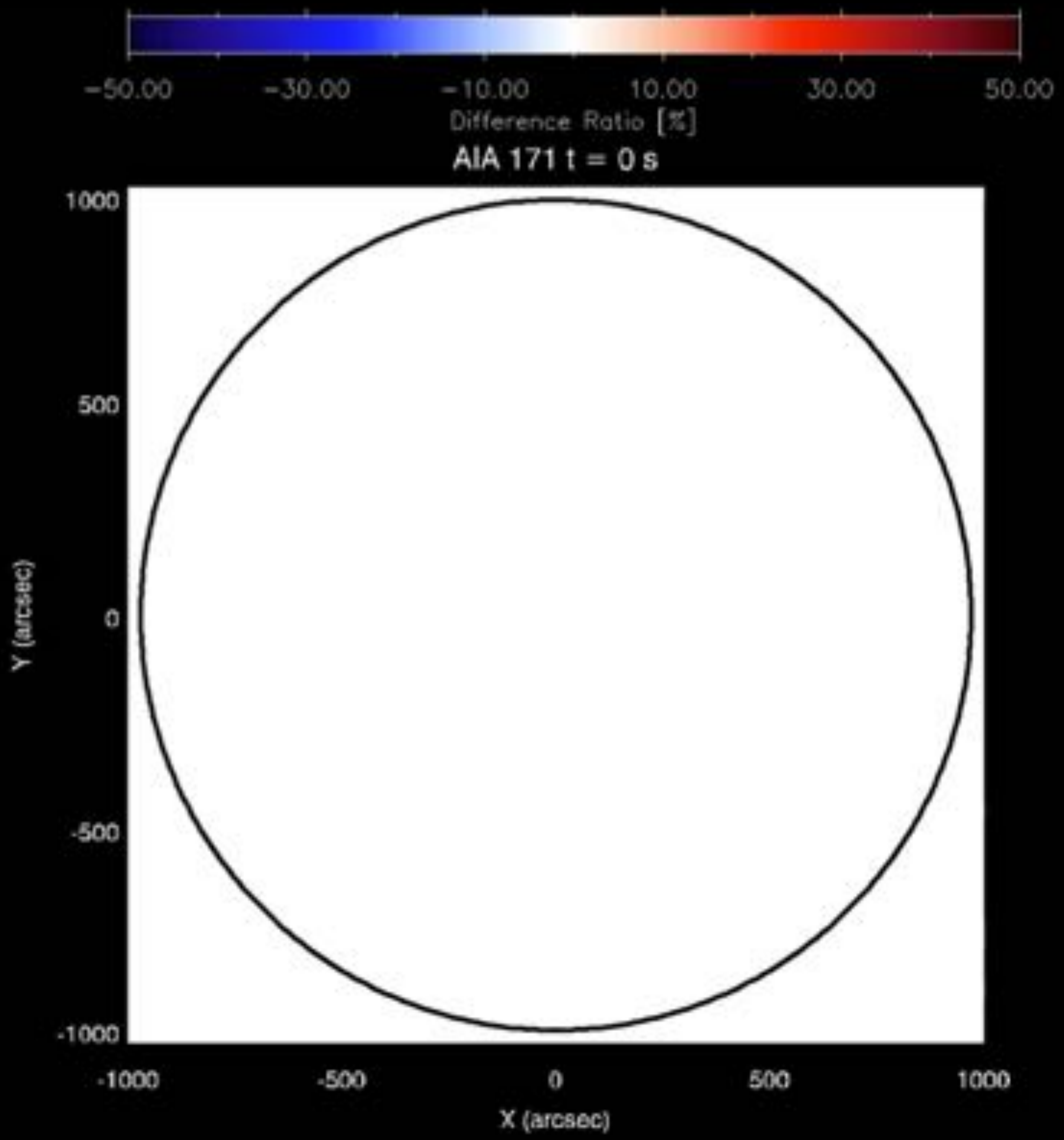

AIA 211 (T = 1.86 MK)

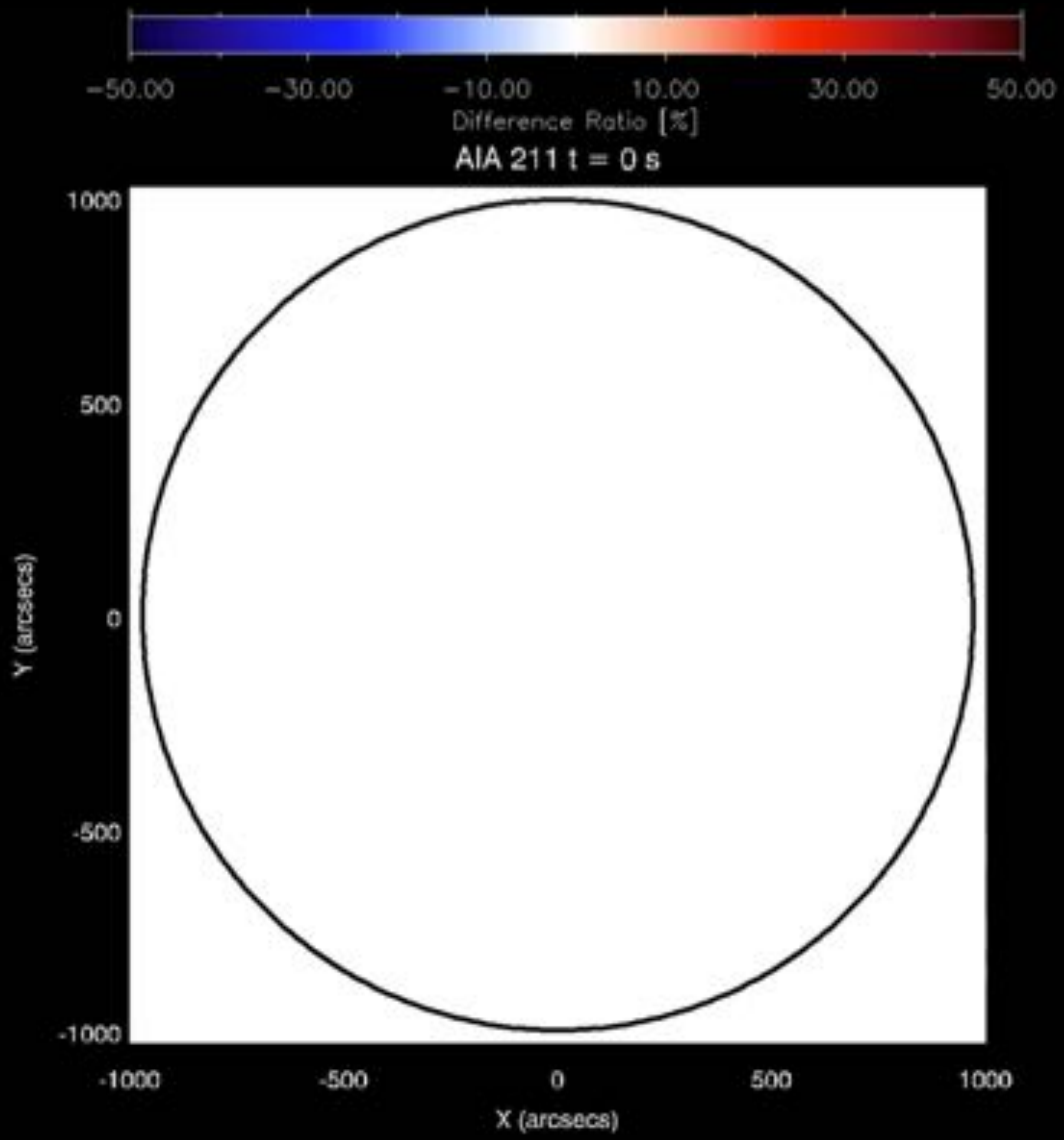

Core Dimming

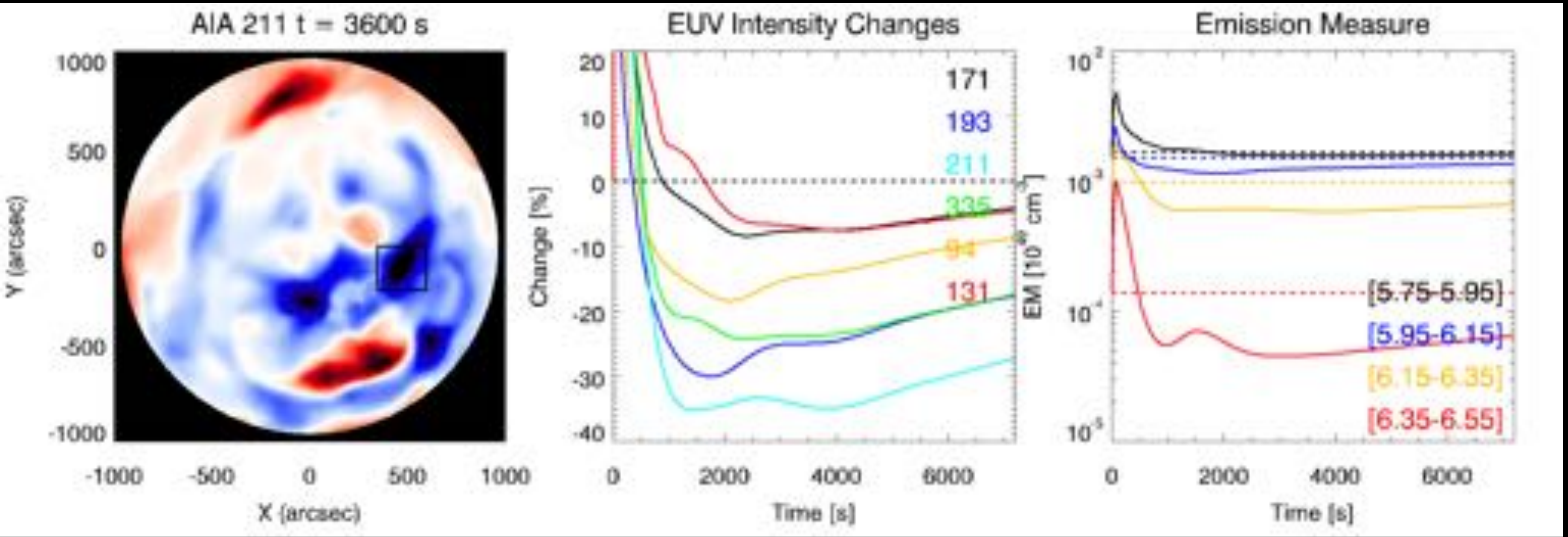

- **Emission Measure (EM)** calculated from the simulation data.
- **Core Dimming** (near the source region): Plasma depletion induced by CME.
- Dimming recovery time is estimated **~9-16** hours.

Remote Dimming

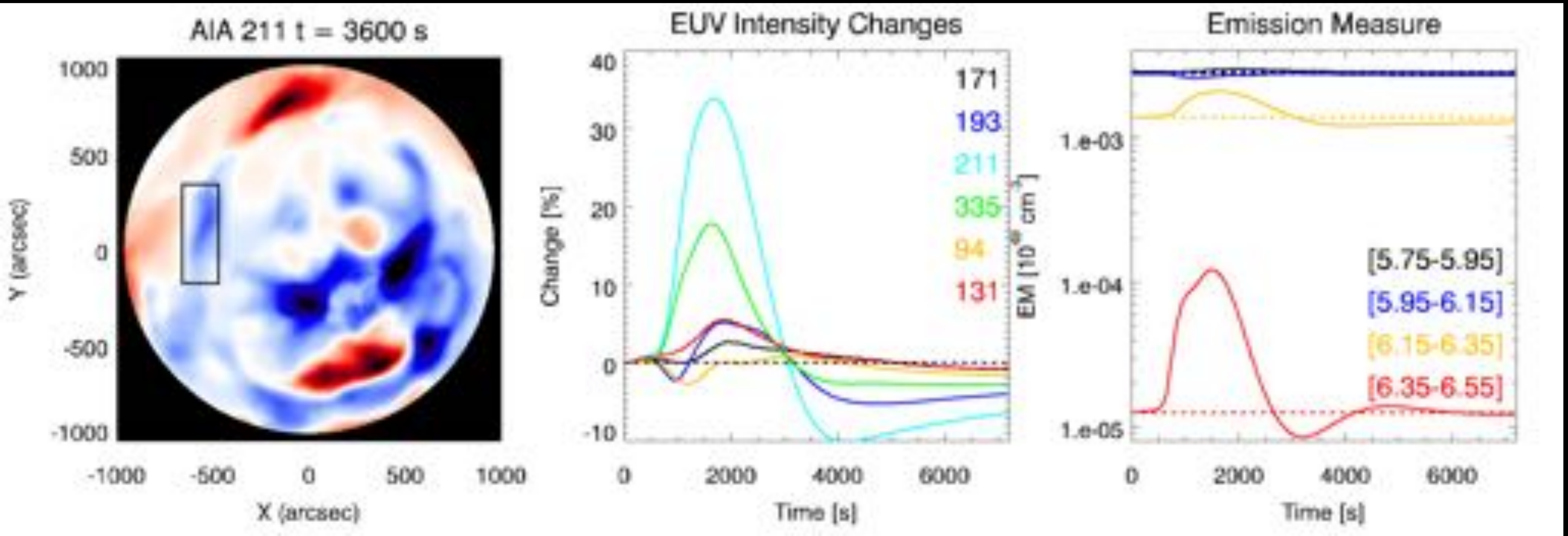

- **Thermal Dimming / brightening** due to the plasma compression during the eruption phase.
- Dimming during the recovering phase corresponding to the open field region.

Dimming Slope/Depth vs. CME Speed/Mass

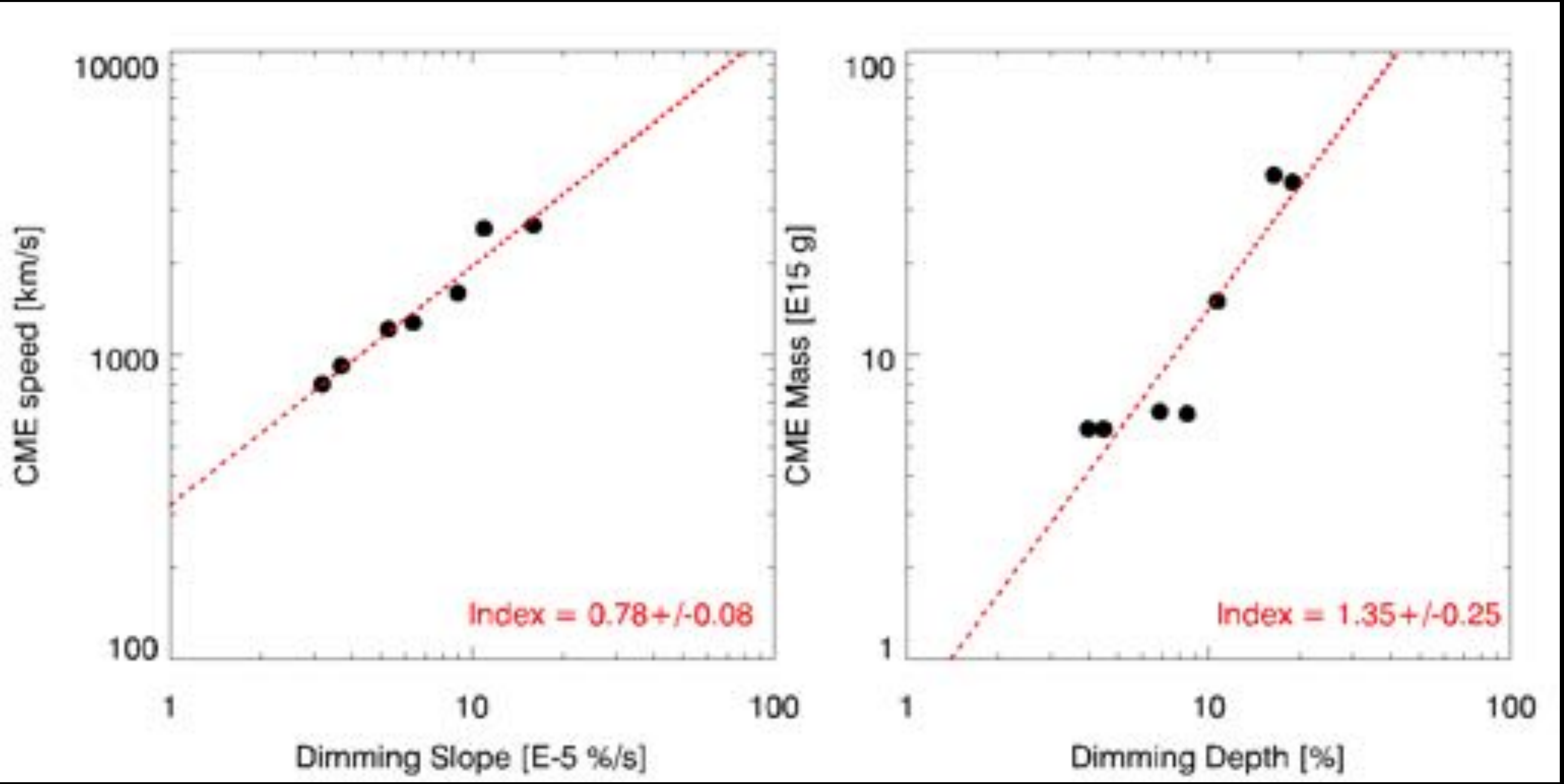

- Note that the simulation runs involve different flux rope energies and flux rope orientations.
- The simulation result is consistent with the findings of *Mason et al. (2016)* using SDO/EVE observations and *Dissauer et al. (2018)* using SDO/AIA observations.
- The relationship can be used to estimate the CME speed and mass at the early stage of the eruption.

CME-driven Shocks (2011 March 7 Event)

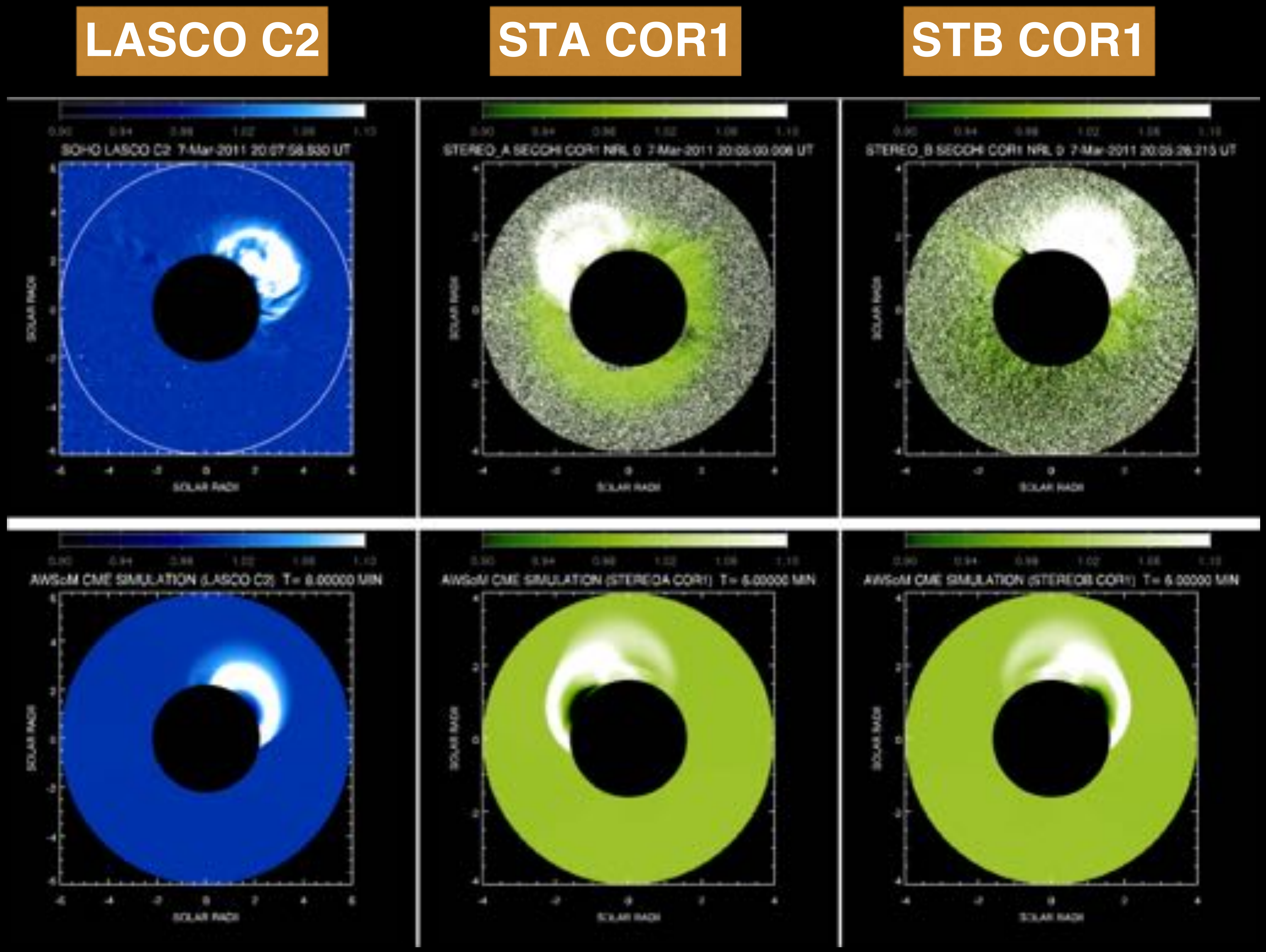

CME-driven Shocks (2011 March 7 Event)

Shock Evolution in the Simulation

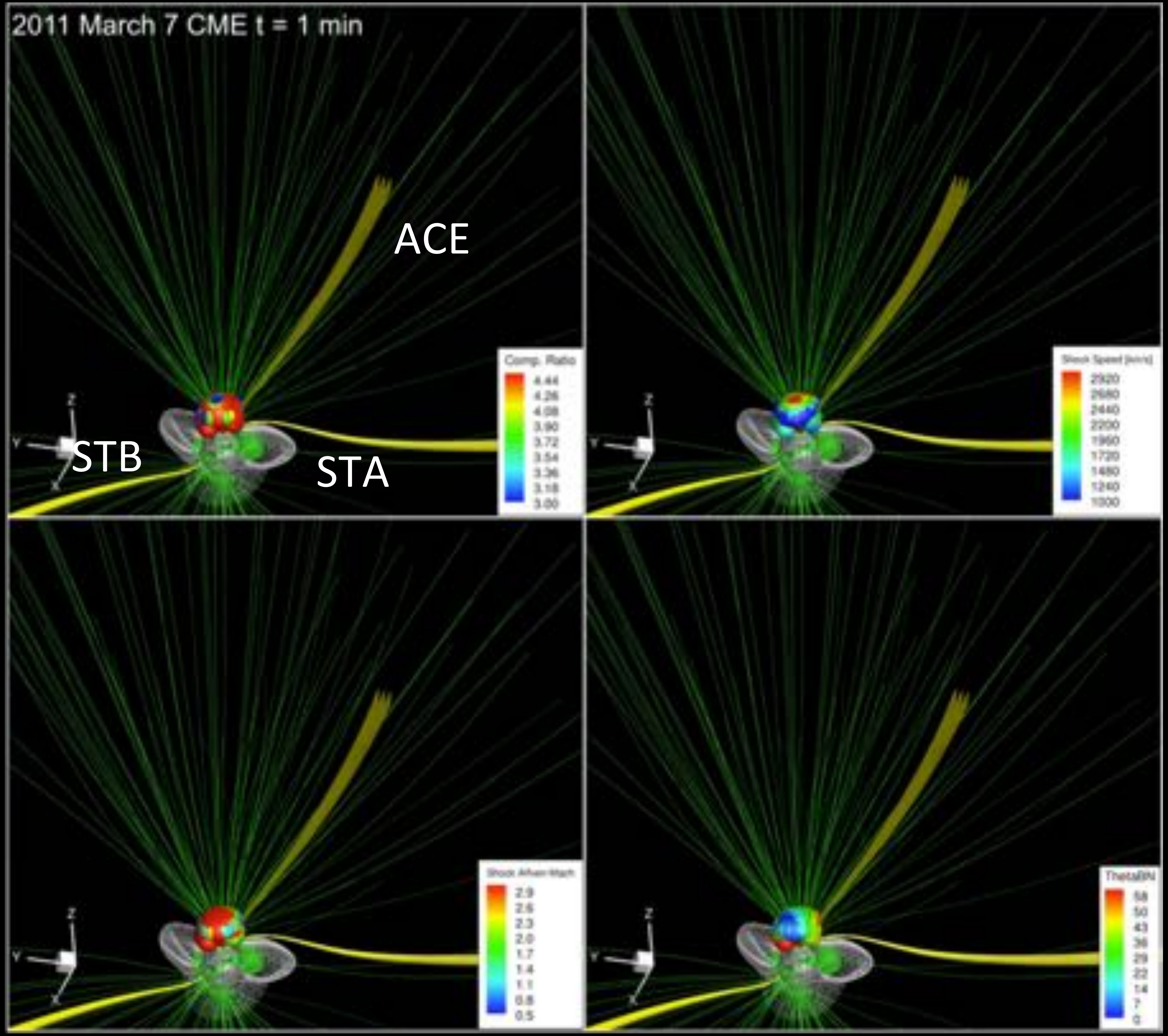

Shock Parameters from Observation

Kwon et al. 2018

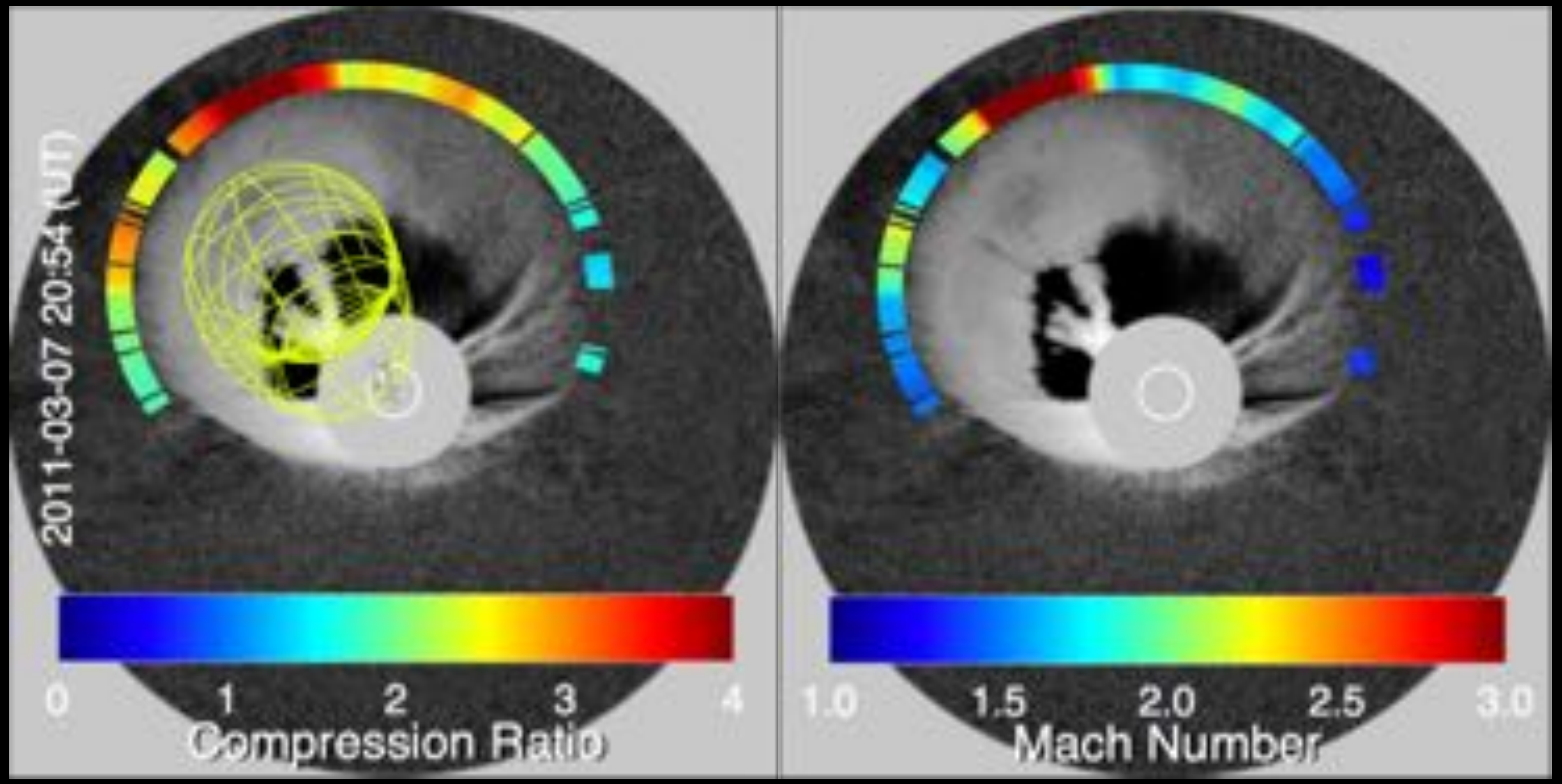

Shock Parameters from Simulation

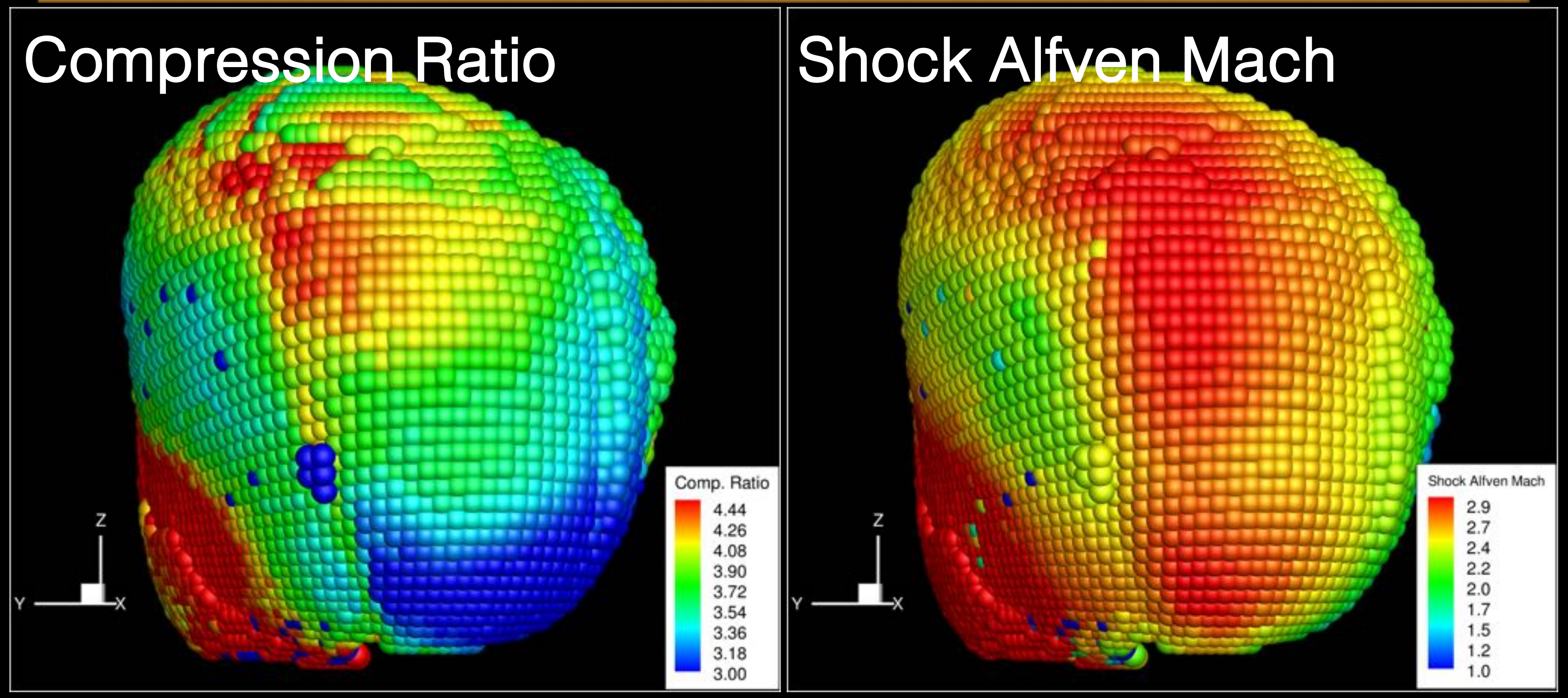

SEP Observation and Q/A Analysis

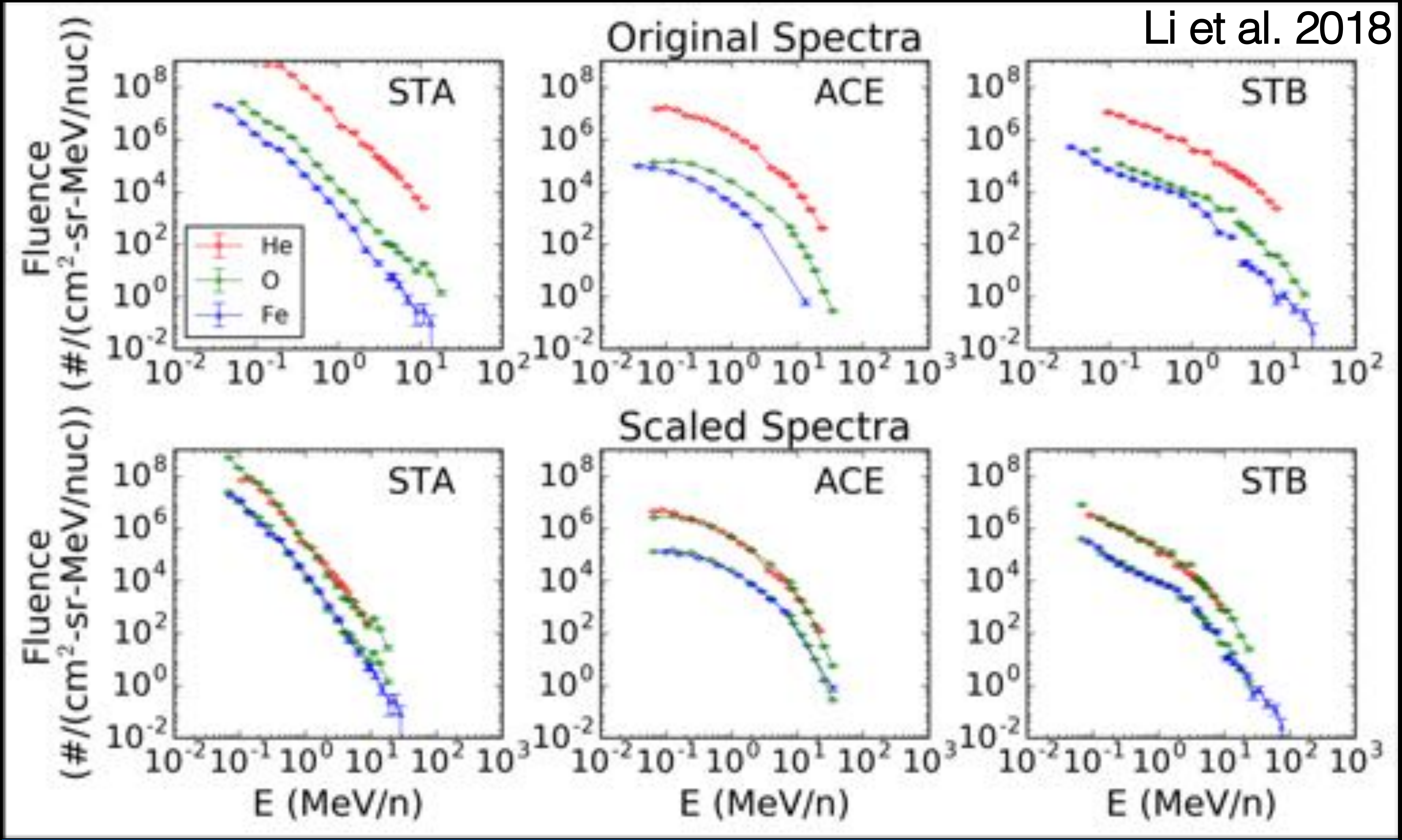

$$\frac{(Q/A)_i^\sigma}{(Q/A)_O^\sigma} = \frac{E_i}{E_O}$$

- The Q/A analysis (Li et al. 2009, Zhao et al. 2016) suggests that the shock connecting to ACE is most parallel, STB is quasi-parallel but more oblique.
- Event integrated spectra at STA are very power-law-like, showing no clear scaling. Further examination of STA data shows that there were a CIR at STA, which interacts with the CME (and its driven shock).

Li et al. (2009) attempted to relate sigma to shock geometry. They showed that the value of sigma is usually in the range of 1 to 2 for parallel shocks, but can become as small as 1/5 for perpendicular shocks.

- **ACE** connects to the CME-driven shock earlier than STA and STB.
- Both **STA** and **STB** start to contact with the CME-driven shock around **t=2 hours**.
- **ACE** connects to **a quasi-parallel shock** geometry, **STB** more **oblique**, and **STA** likely to a **quasi-perpendicular shock**.

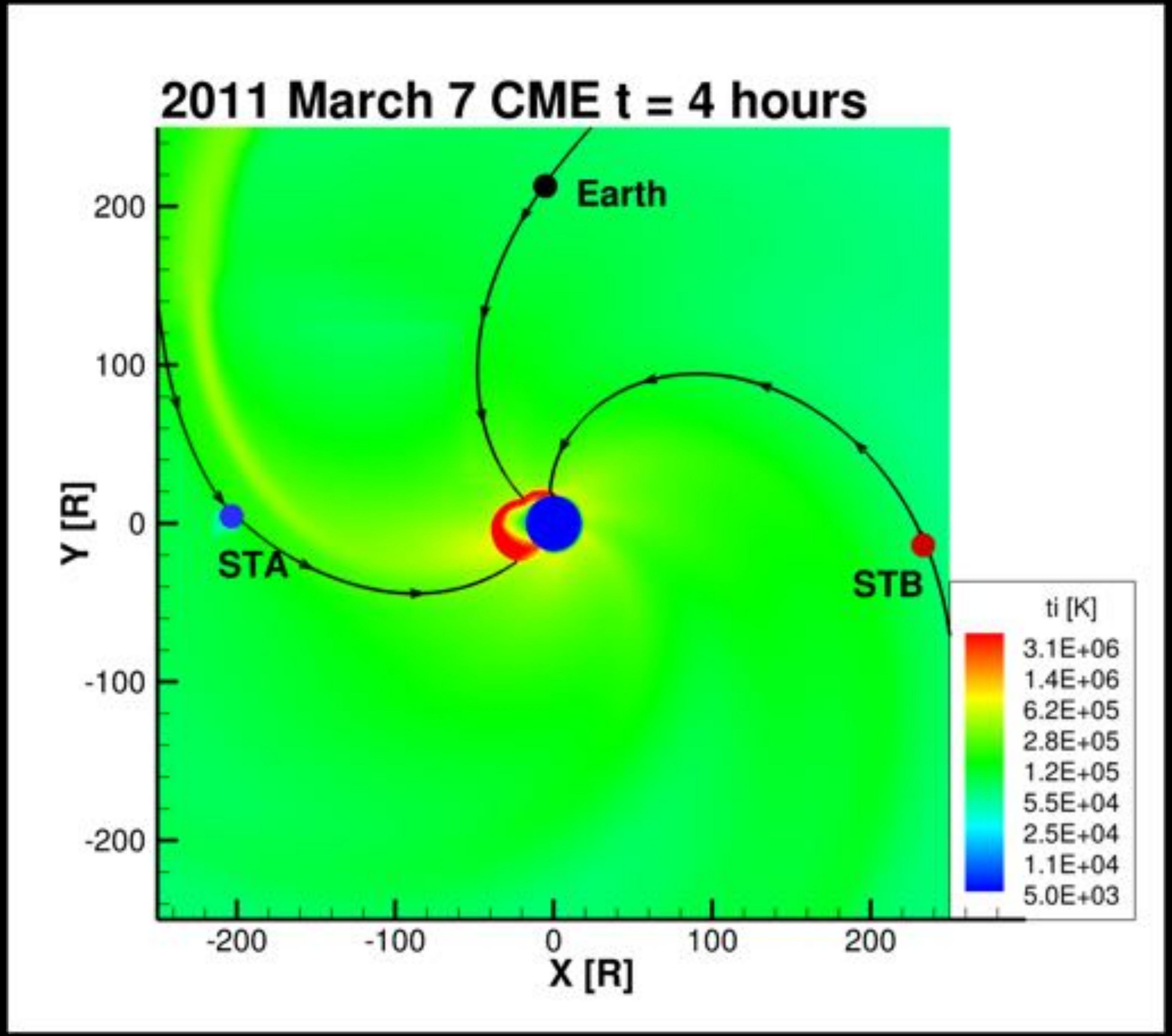

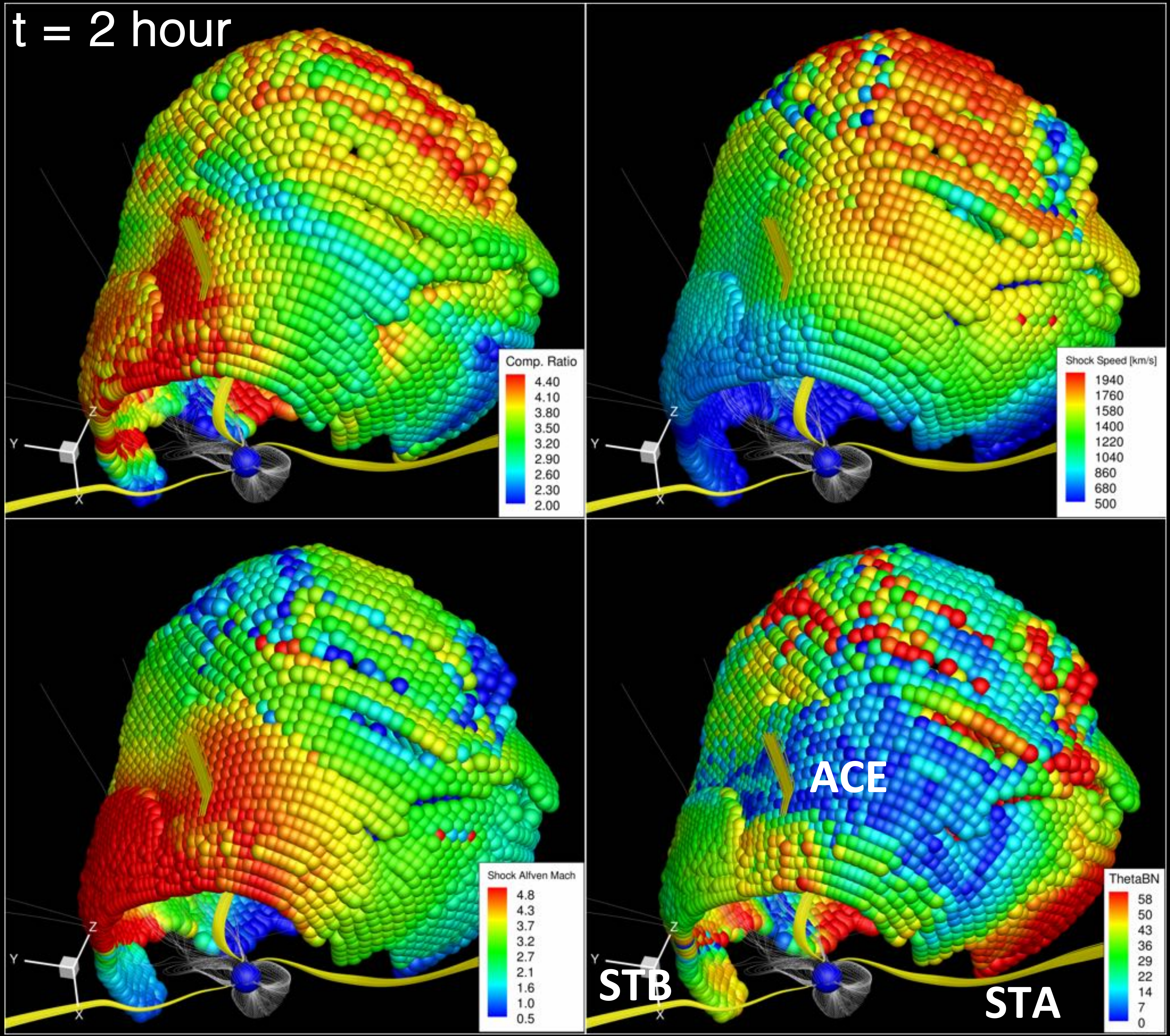

Fermi Behind-the-Limb Event on 2014 September 1

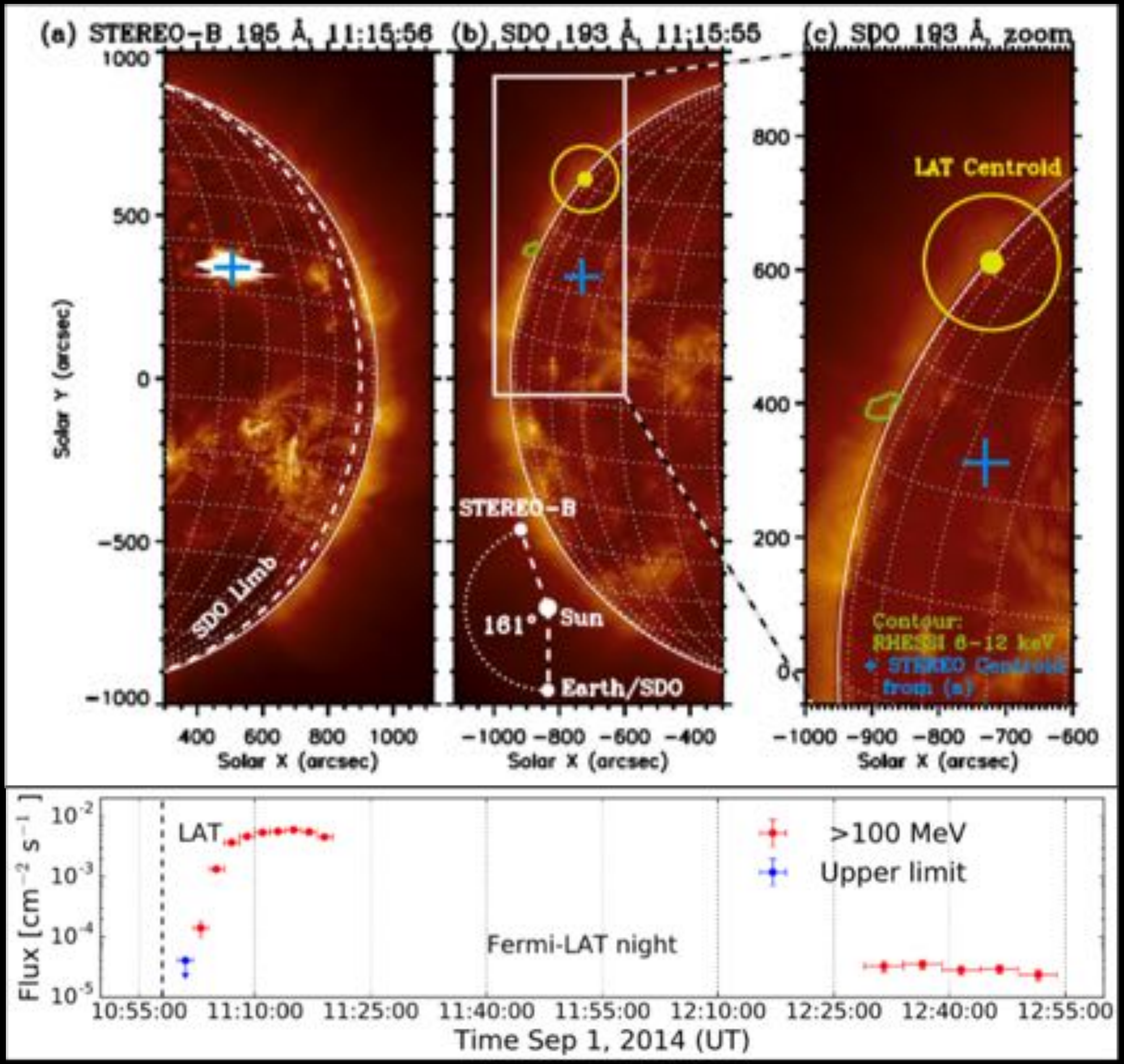

Ackermann et al. 2017

- Behind-the-limb (BTL) gamma-ray flares (up to 100 MeV) were observed in solar cycle 21 and 22 (Vestrand & Forrest 1993, Barat et al. 1994, Vilmer et al. 1999).
- There are 3 behind-the-limb (BTL) flares with E>100 MeV observed by Fermi-LAT so far:
  - 2013 October 11 (located ~10 degree behind the eastern limb)
  - 2014 January 6 (located ~20 degree behind the western limb)
  - 2014 September 1 (located ~43 degree behind the eastern limb)
- Fermi-LAT detected emission from this flare on the front side of the Sun for ~2 hr, peaking between 11:10-11:15 UT.
- The September 1 event is also associated with a fast CME with a speed > 1900 km/s. A Type II radio burst was also detected with an estimated velocity of 2079 km/s (Pesce-Rollins et al. 2015).
- Cliver et al. (1993) first proposed that the BTL gamma-ray events are caused by particles that are accelerated at CME-driven shocks and then propagate back to the visible solar disk.

When, where, and how the particles are accelerated?
What is the role of CME?

CME-driven Shock Evolution (Earth View)

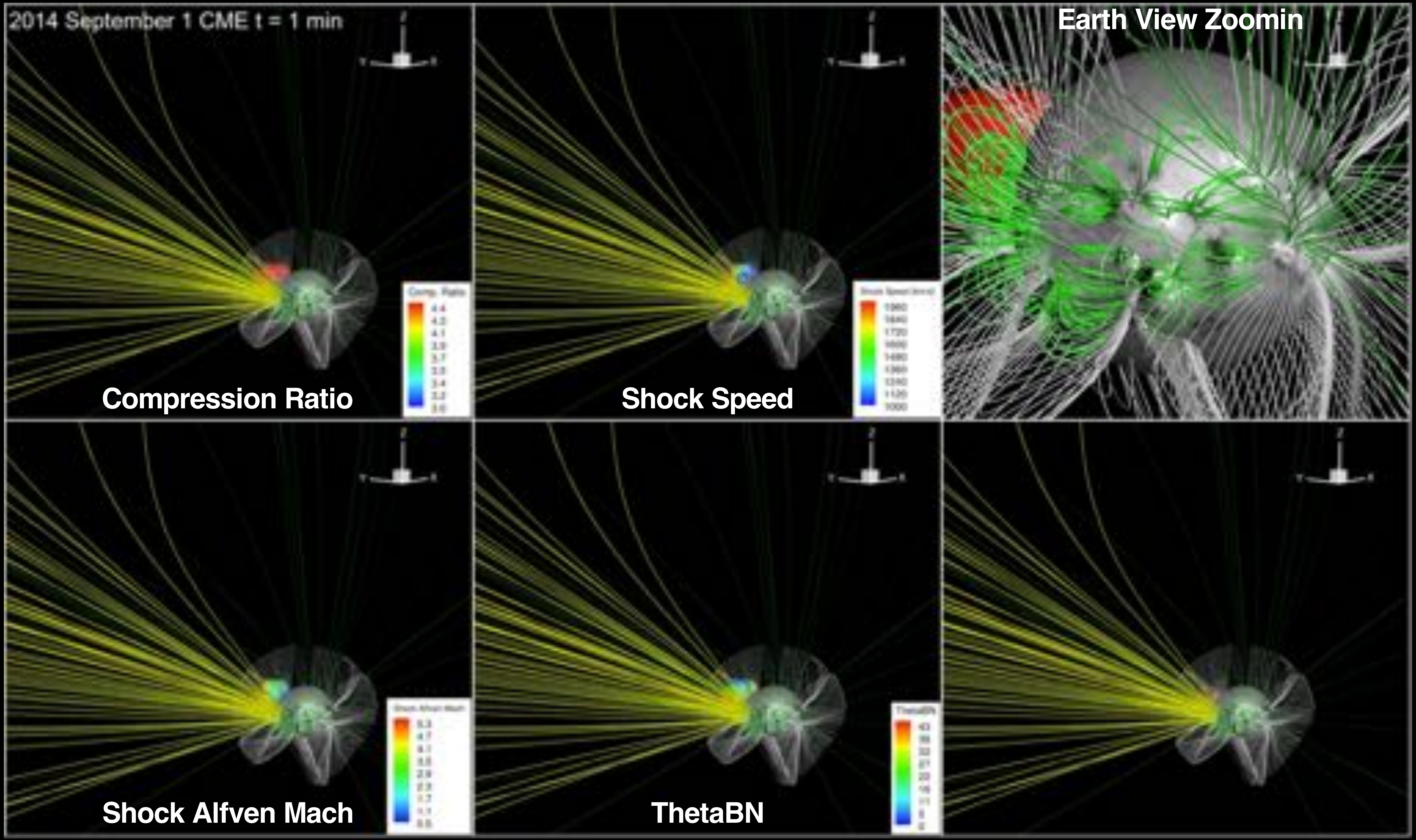

Yellow:
Open field near the Fermi-LAT Gamma-ray emission region connected to the CME-driven shock.

Red :
Flux Rope field lines

White :
Large-scale helmet streamers.

Green:
Surrounding active regions and open field lines.

Shock Parameter Evolution

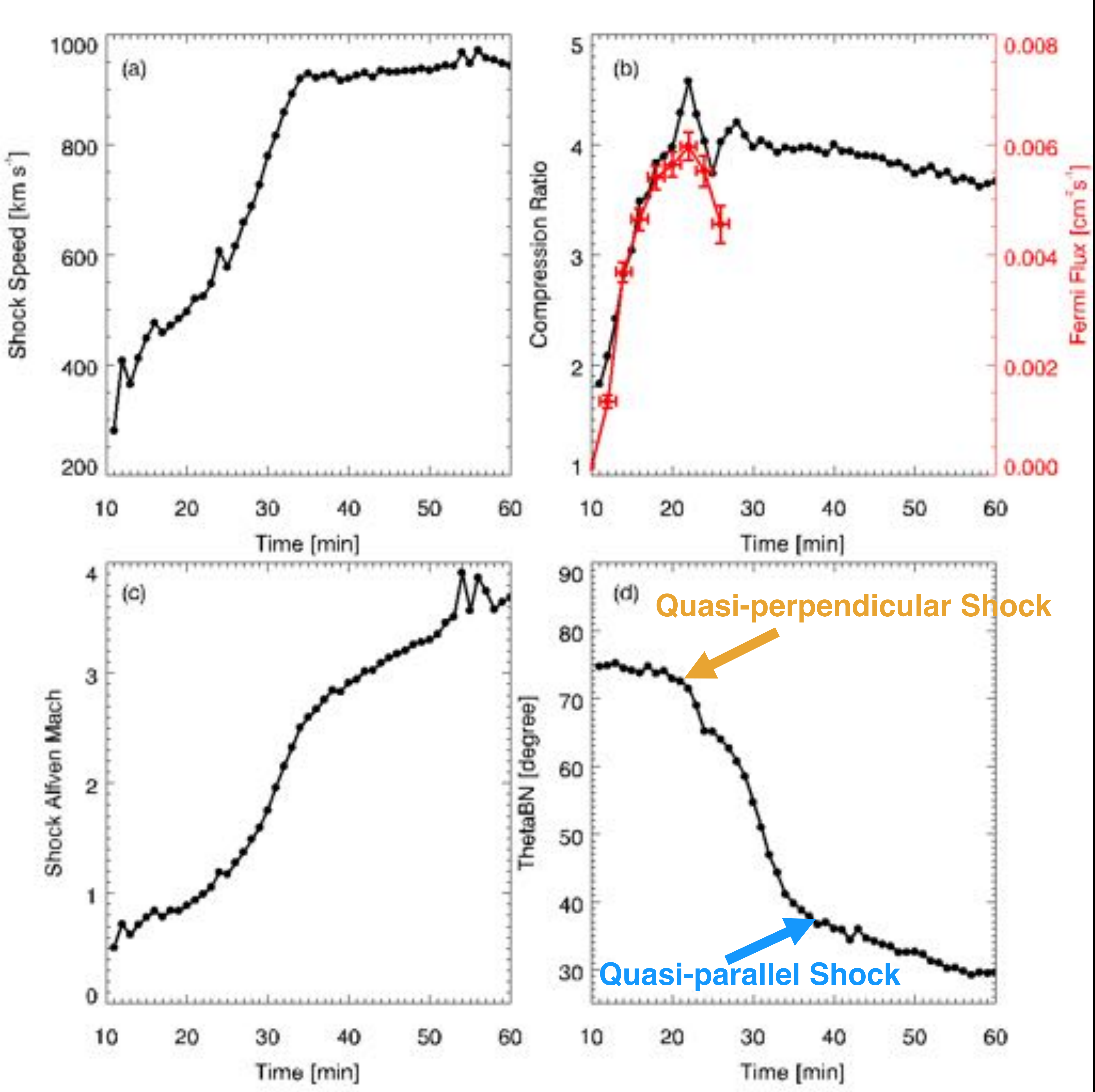

- We obtain the shock parameters averaged over the portion of the **shock surface that is connected back to the visible side of the Sun** and track their temporal evolution.
- Shock compression ratio increases rapidly from ~1.8 at 10 minutes to ~4.6 at 20 minutes and then gradually decreases to ~3.7 at 60 minutes. This evolution trend is similar to the Fermi/LAT gamma-ray intensity profile (Ackermann et al. 2017).
- The shock changes from a quasi-perpendicular shock (before t= 30 minutes) to a quasi-parallel shock at t = 60 minutes.
- The mirror ratio (B_sun/B_shock) in the simulation is ~10 to ~100 within 1 hour, which suggests a large fraction of the downstream GeV protons can reach the photosphere within the emission duration (Petrosian 2016).

Jin et al. 2018, ApJ, in press

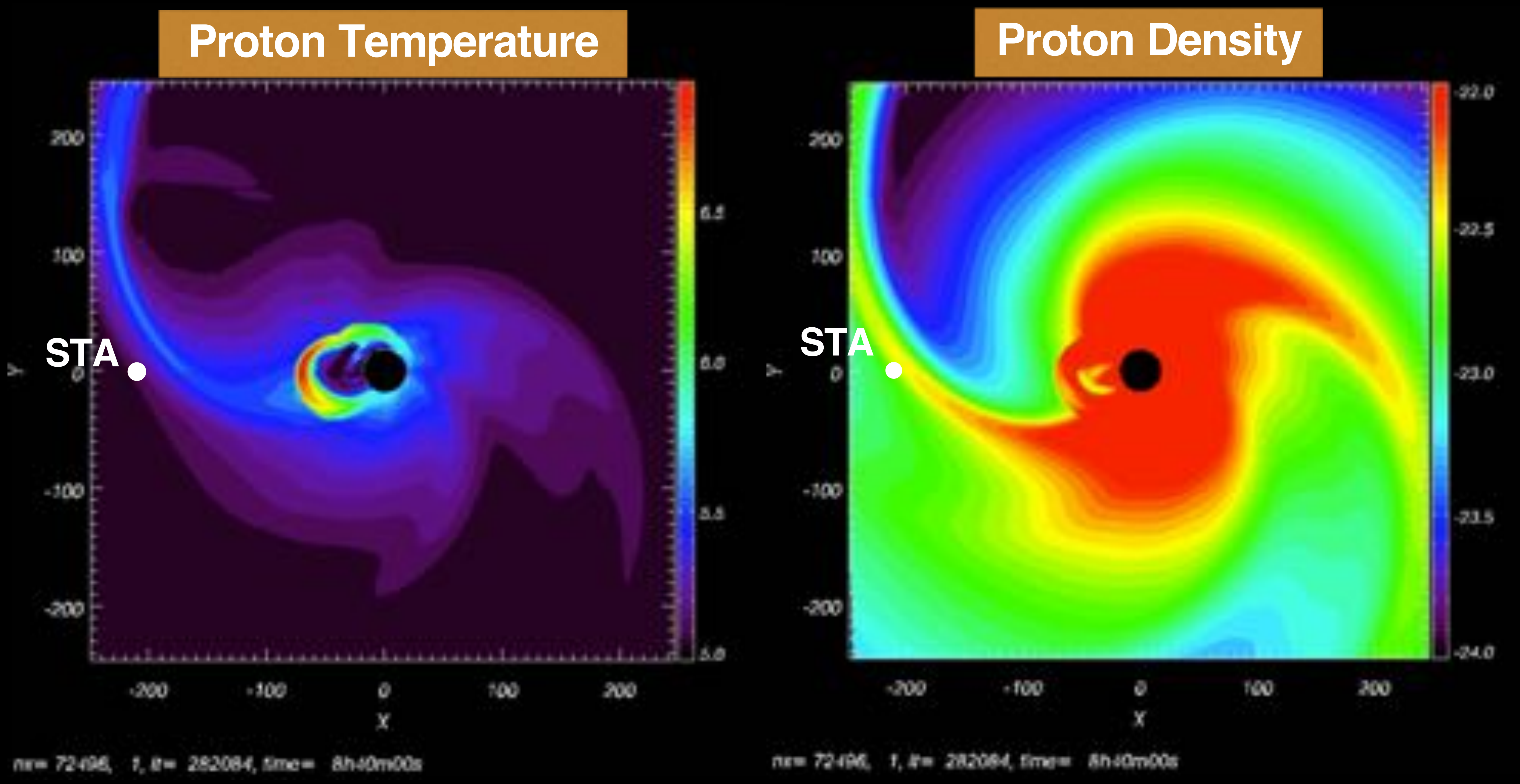

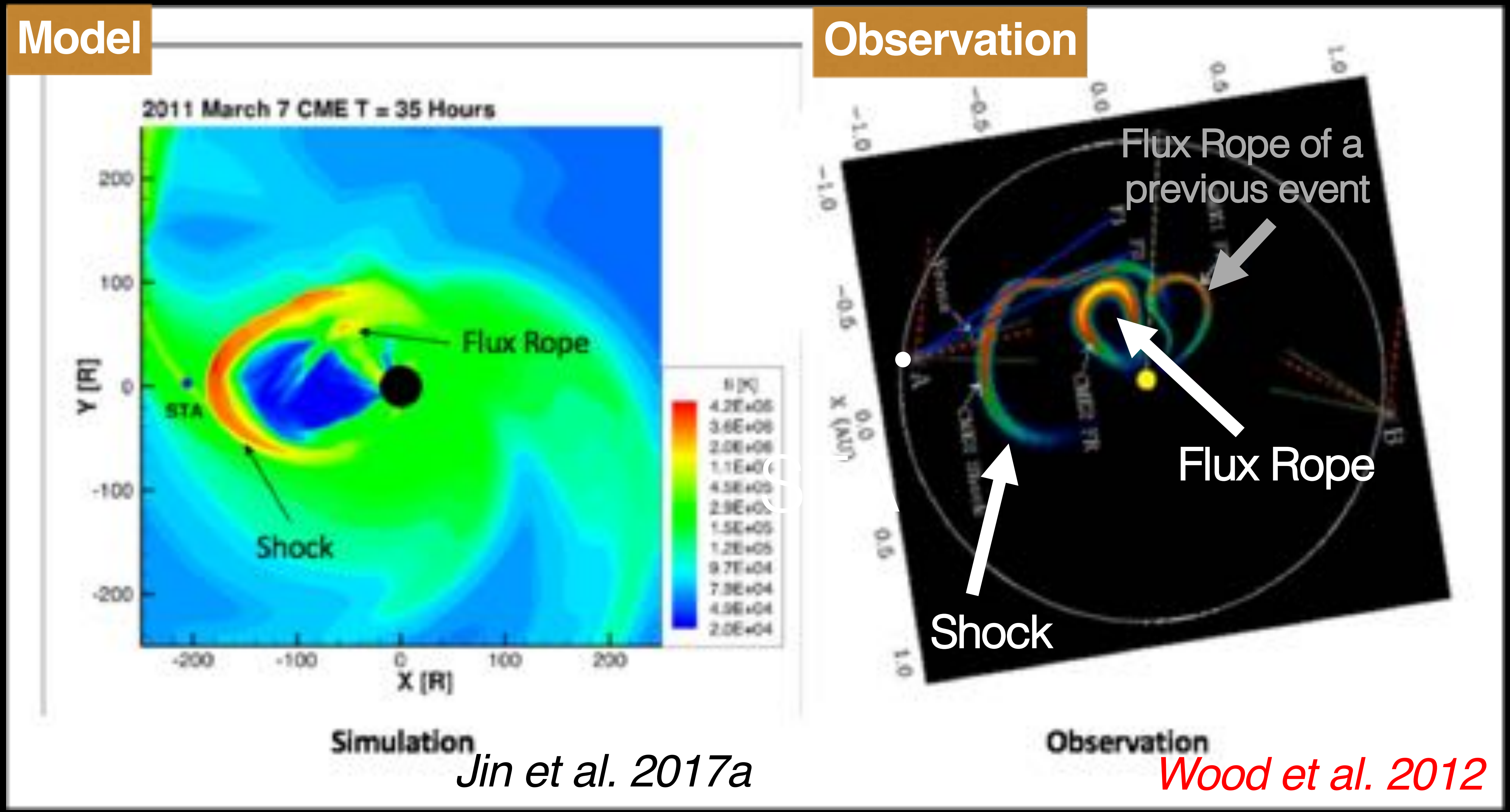

Jin et al. 2017a
Wood et al. 2012

CME Evolution in the Heliosphere (2011 March 7 Event)

- The **shock-CIR interaction** acts as shock-shock collisions (e.g., CME-CME interaction; *Lugaz et al. 2008, Shen et al. 2011*) and will amplify the magnetic fields, plasma temperature, and density of the CIR.

- **CME deflection** (e.g., *Gopalswamy et al. 2009, Lugaz et al. 2011, Kay et al. 2013*): Evident both in the observation and in the simulation. The CME-driven shock expands into the coronal hole's fast outflow and travels far from the ejecta where it is observed by STA.

- Although initially **driven by the CME flux rope** close to the Sun, the shock toward STA becomes detached from the driver in the heliosphere and has features similar to a **blast wave**, which is consistent with observations (*Wood et al. 2012*).

1 AU Comparison (2011 March 7)

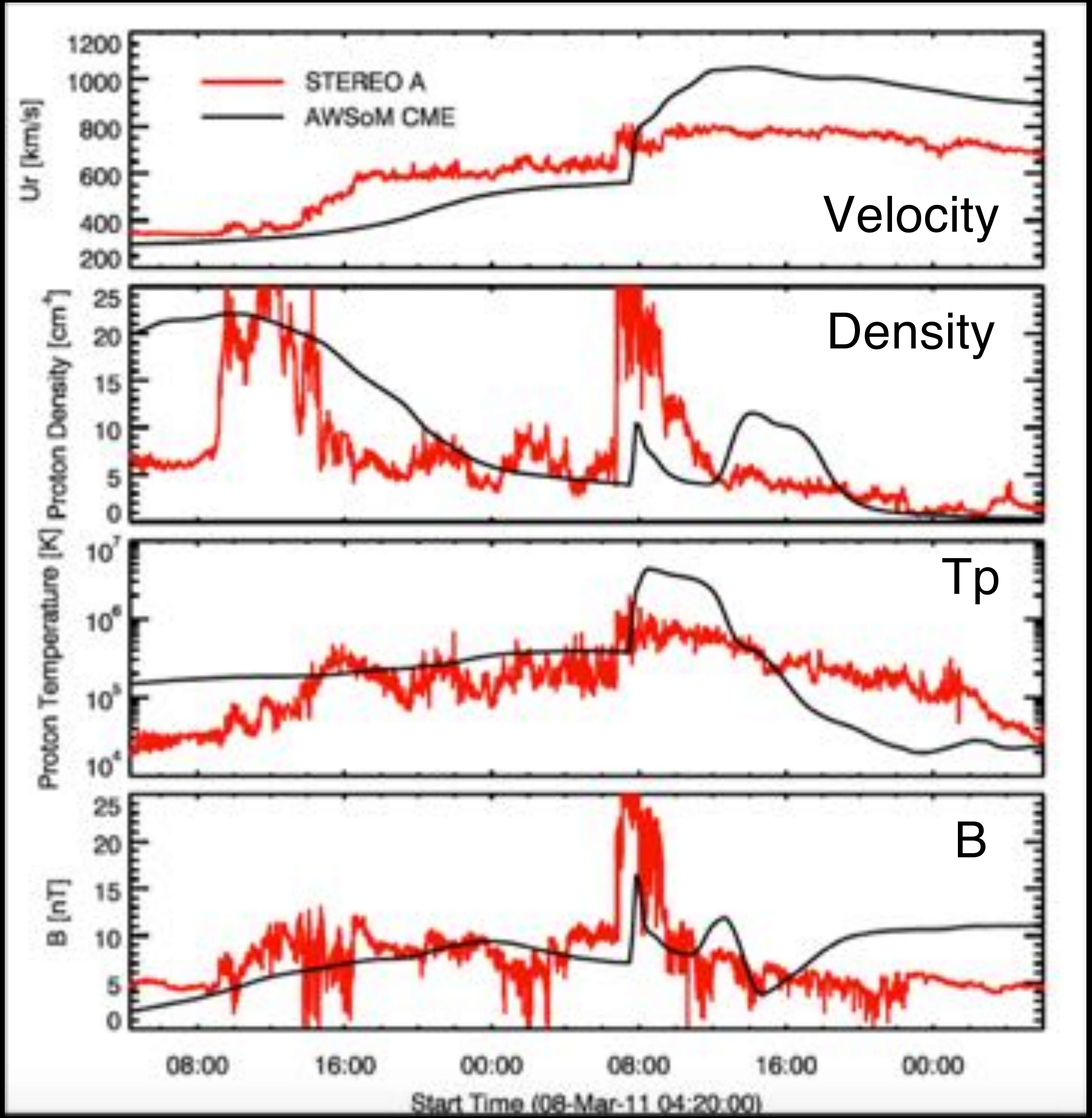

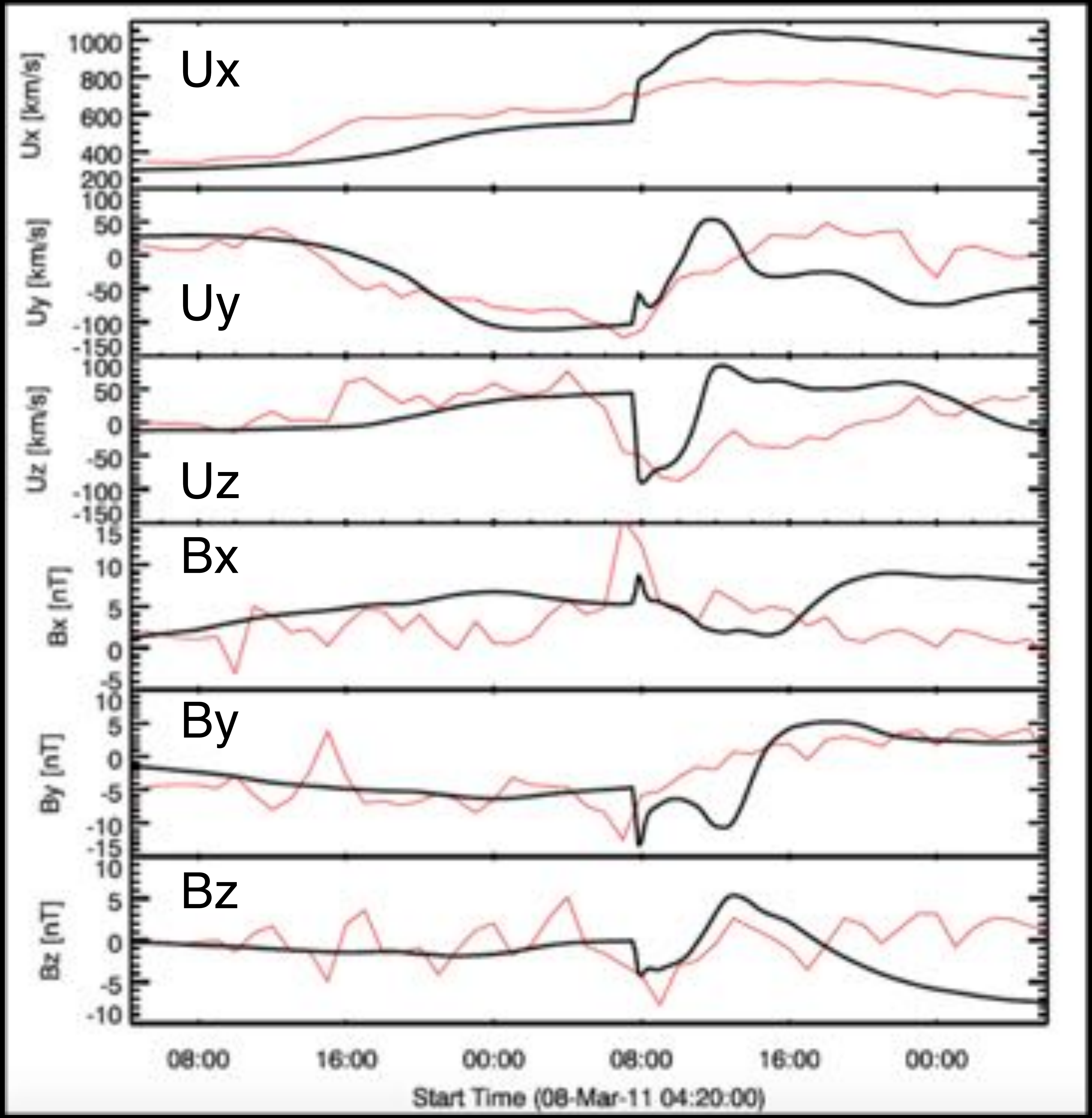

Jin et al. 2017a

EEGGL: Eruptive Event Generator (Gibson and Low)

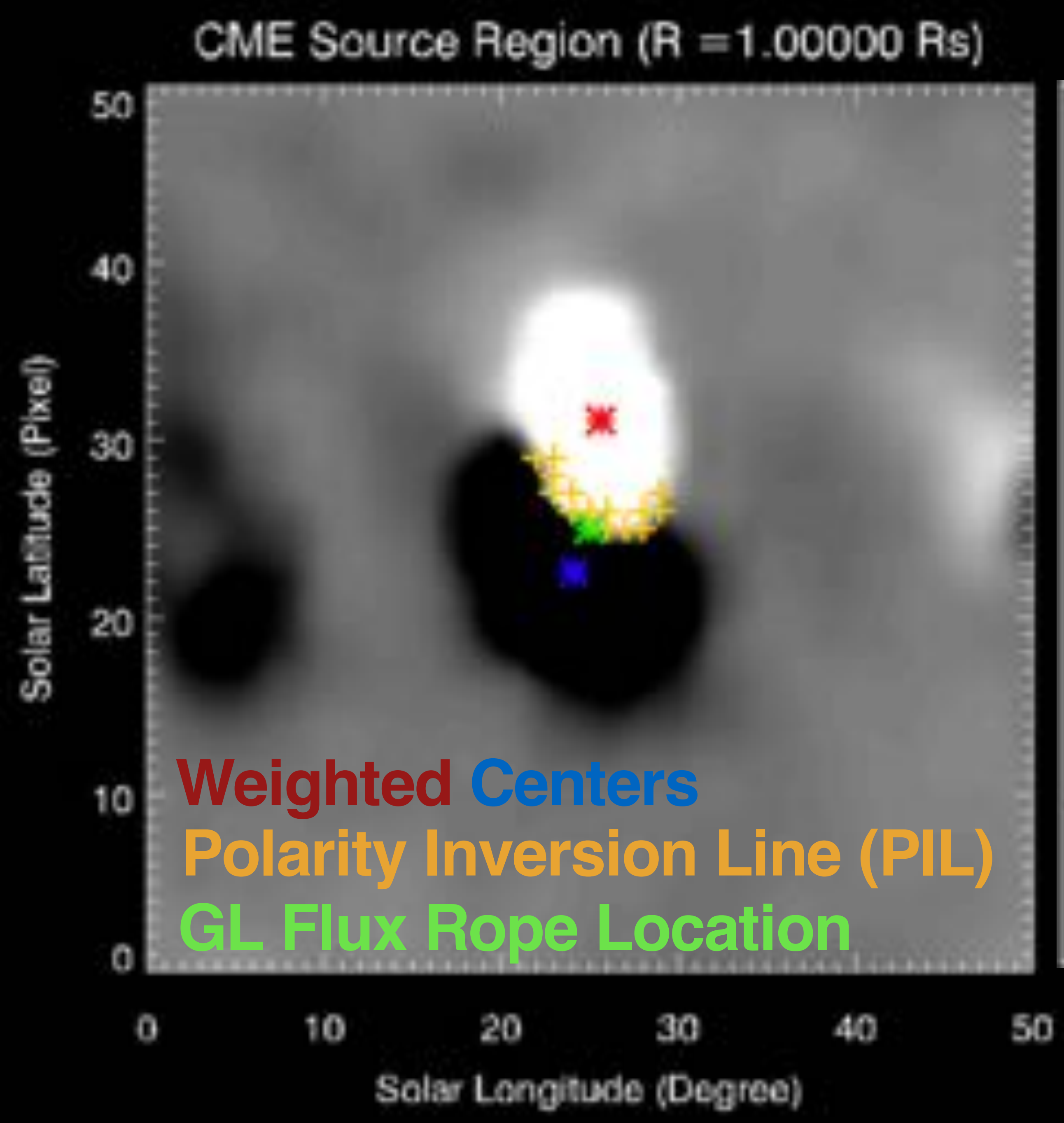

GL 3D Configuration

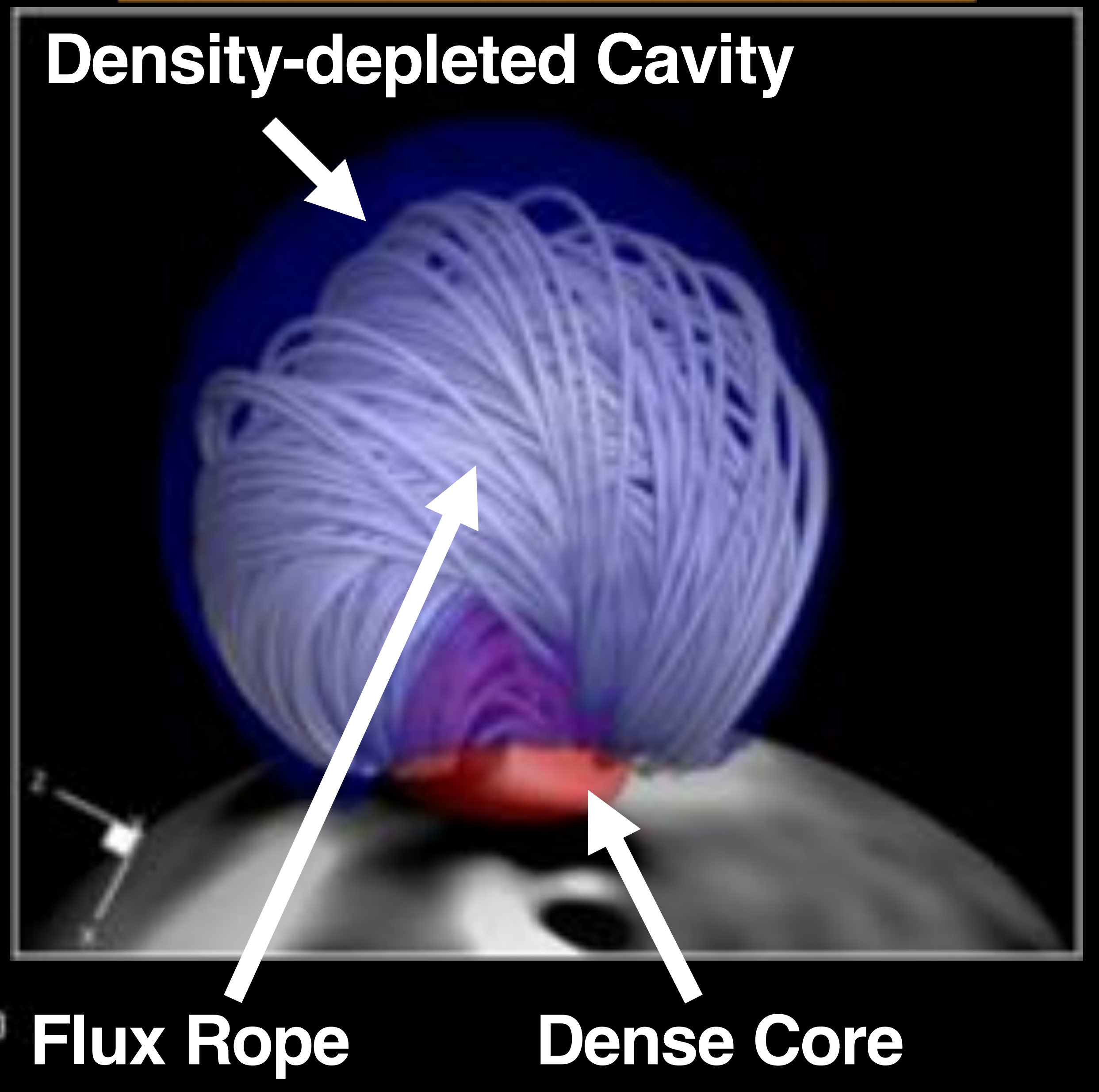

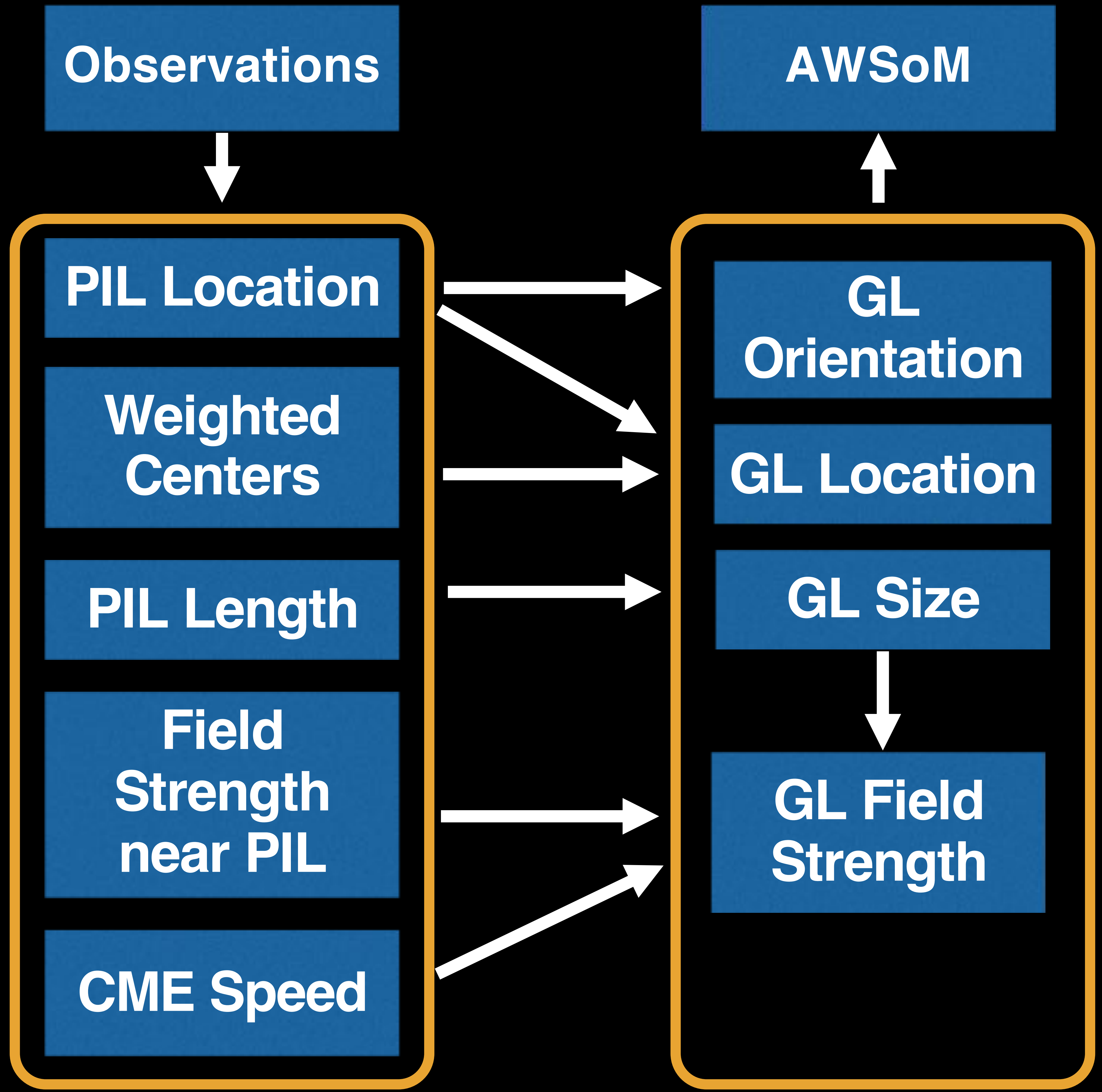

- **EEGGL uses observational data to specify input parameters for the Gibson-Low flux rope model (Gibson & Low 1998) so that it may approximately reproduce observed CME events.**

(Jin et al. 2017b)

More information: https://ccmc.gsfc.nasa.gov/eeggl/

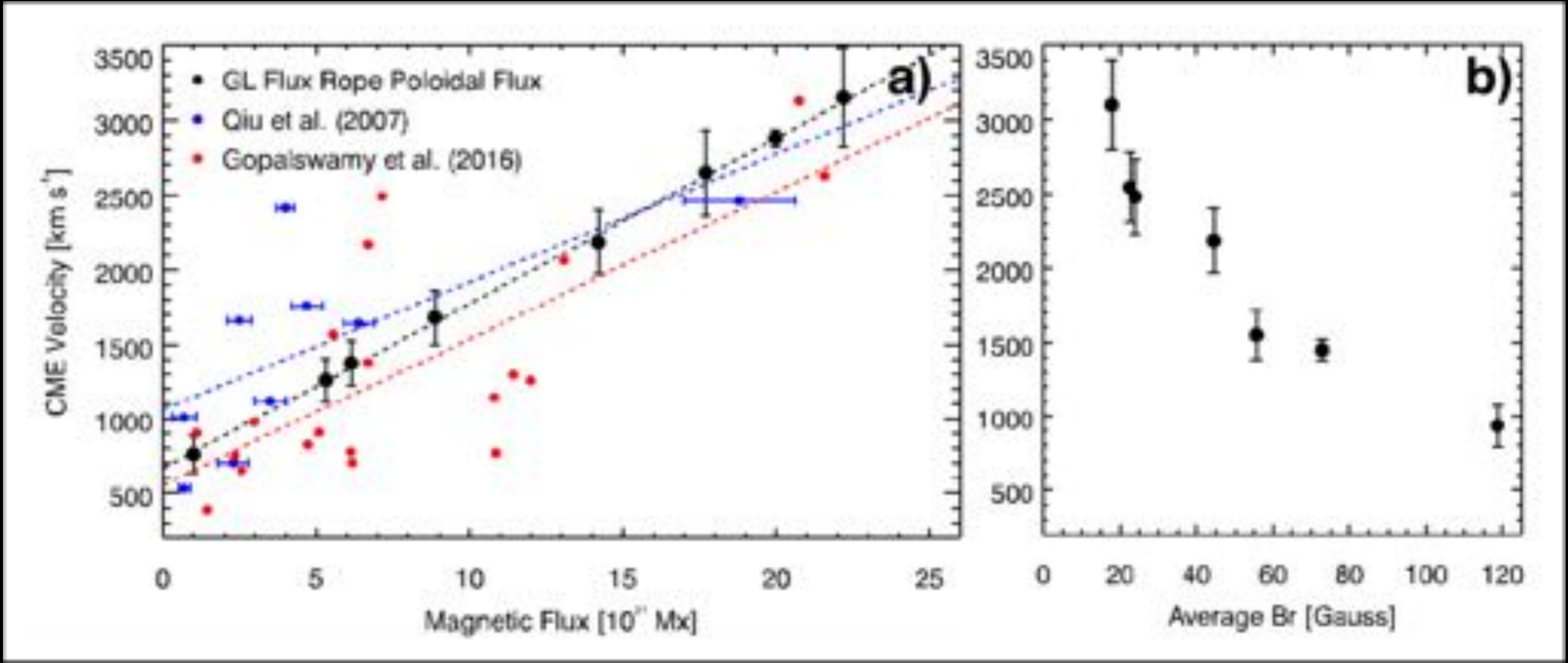

- With different GL radius/strength parameters, a linear relationship is found between the flux rope **poloidal flux** and the **CME speed** near the Sun.

- With the same flux rope parameters, the **CME speed** is inversely related to the **average Br** around the PIL of the active region.

Model Validation & Future Development

2012 July 12 Event Simulation using EEGGL

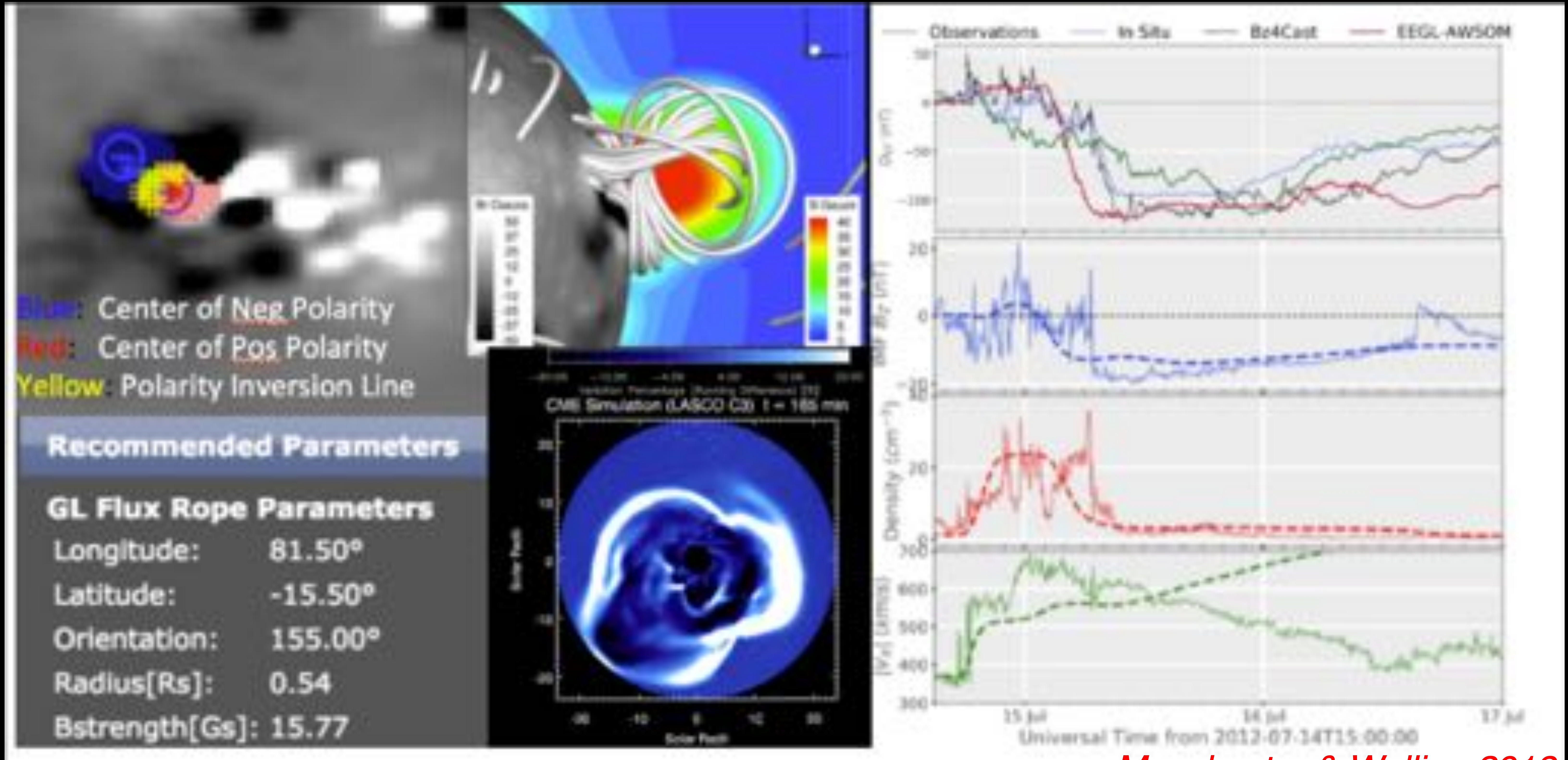

Manchester & Welling 2018

Extensive Events Run

- More validation studies are being conducted at the moment. The results will be used to improve the current EEGGL module.
- New development (e.g., autonomous source region identification) is on-going.

Summary

- The first-principles-based MHD global models play an important role in understanding the fundamental physical processes of CME propagation and interaction in the heliosphere. Although still very challenging, it shows promising potential to provide space weather forecast in the near future.
- Data-driven Models: The flux rope is self-consistently formed in the simulation driven by the electric or magnetic fields from observations (e.g., Cheung et al. 2012, Jiang et al. 2016).
- More Observations:
  - Coronal magnetic field/plasma measurements (erupting flux rope structure)
  - L5/polar mission (more coverage of surface magnetic field)

CME Comparison in White Light

LASCO C2 Observation

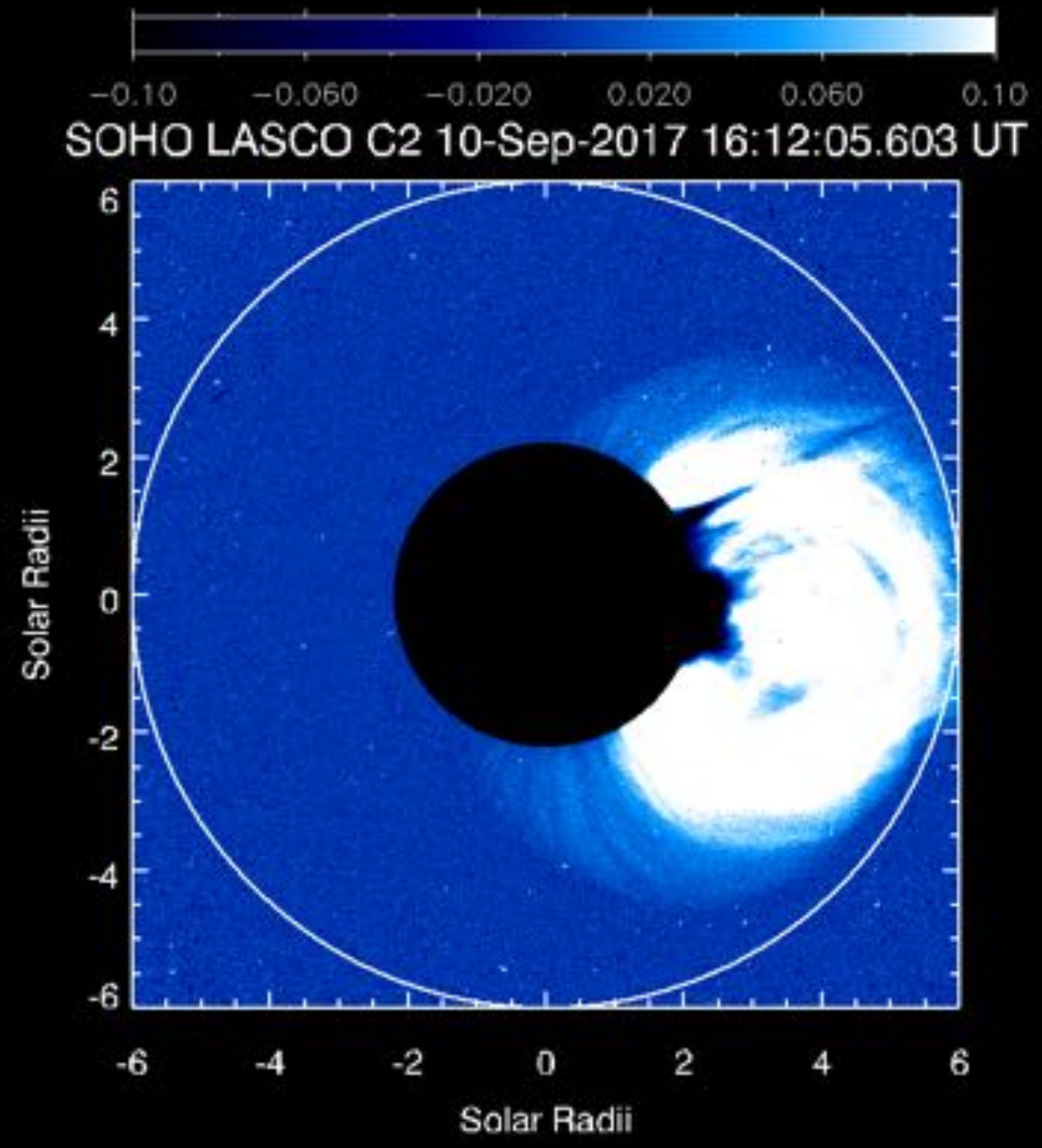

Original Polar Field

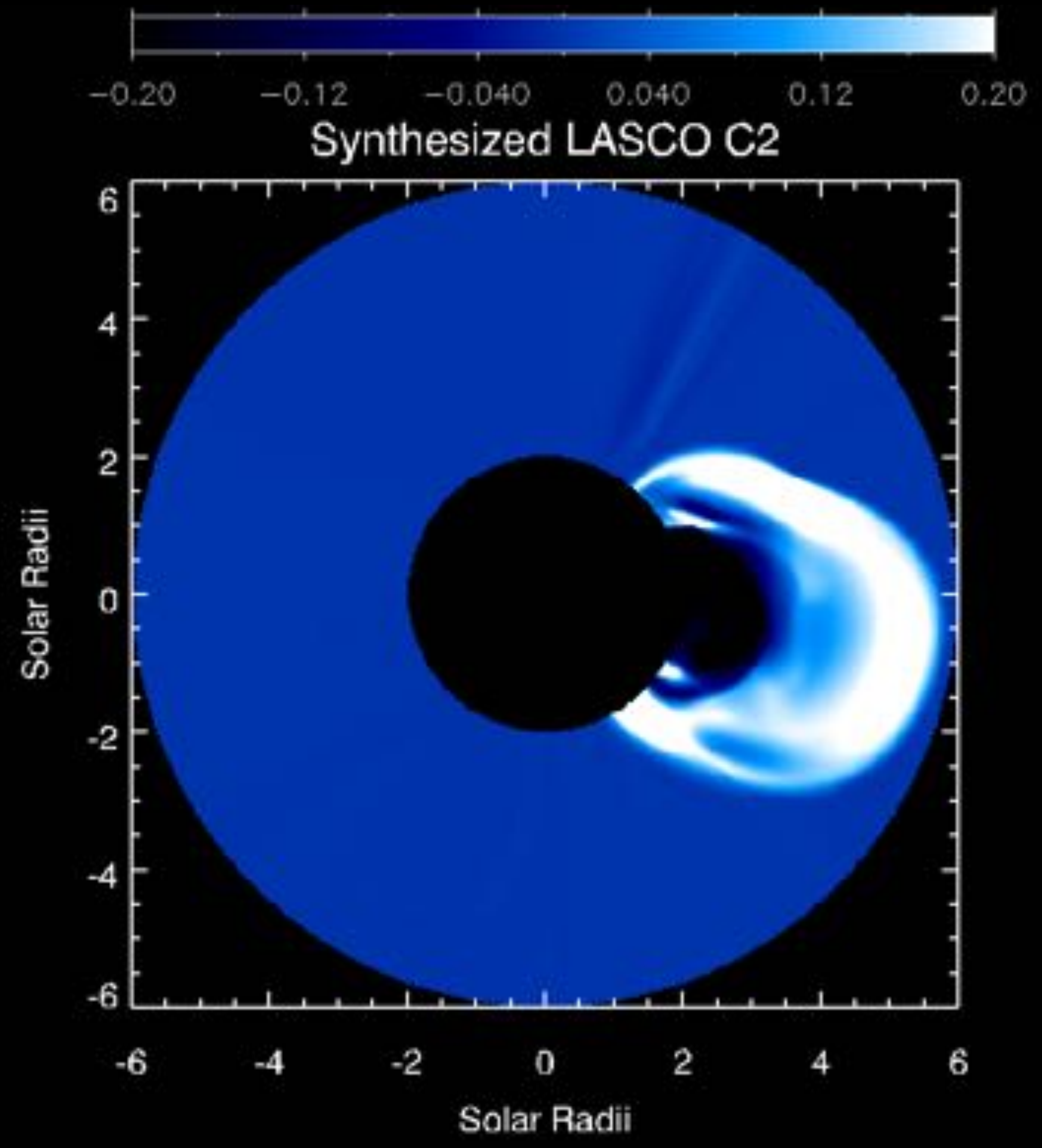

Enhanced Polar Field

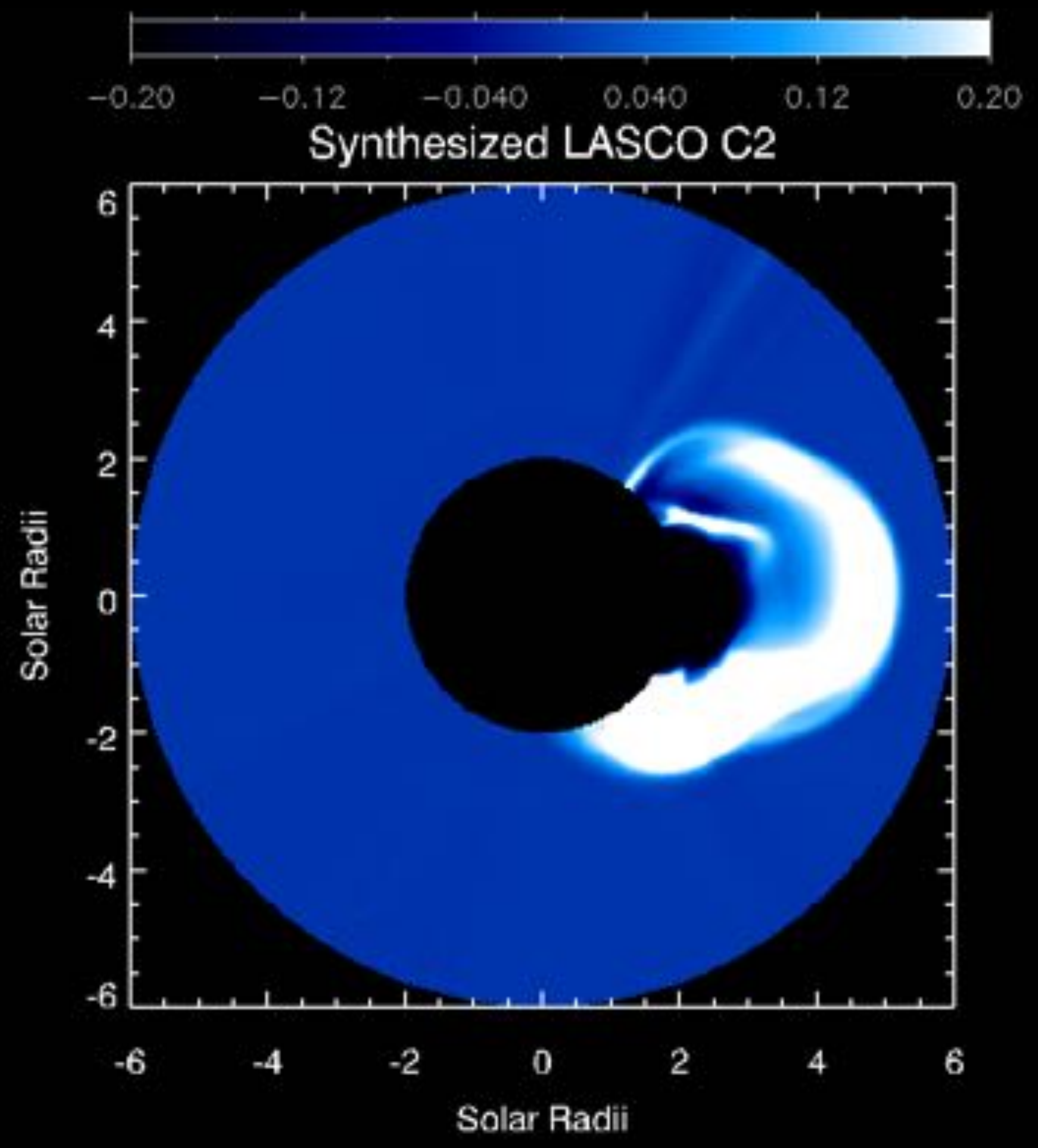

- **With enhanced polar field, the CME direction is changed and more consistent with observation.**
- **The polar field can significantly influence the CME propagation in the simulation. We need accurate polar field observations for better modeling and space weather forecasting.**

Summary

- The first-principles-based MHD global models play an important role in understanding the fundamental physical processes of CME propagation and interaction in the heliosphere. Although still very challenging, it shows promising potential to provide space weather forecast in the near future.
- Data-driven Models: The flux rope is self-consistently formed in the simulation driven by the electric or magnetic fields from observations (e.g., Cheung et al. 2012, Jiang et al. 2016).
- More Observations:
  - Coronal magnetic field/plasma measurements (erupting flux rope structure)
  - L5/polar mission (more coverage of surface magnetic field)
  - Sub-L1 constellation mission (better understanding of magnetic flux rope structure)

Why Multiple in-situ Measurements are Important

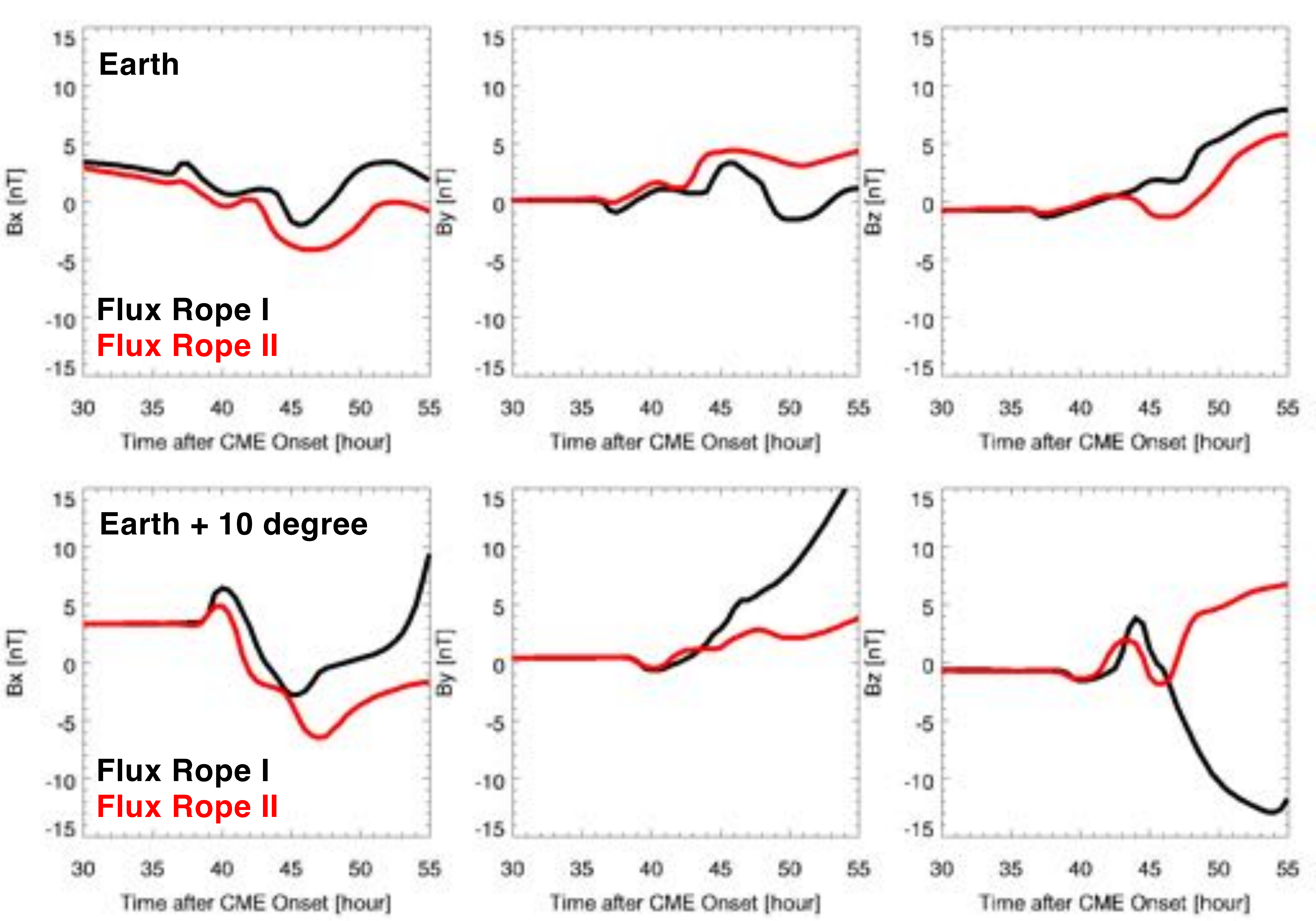

- Global MHD simulation of two flux ropes from the Sun to 1 AU by Alfven wave solar model (AWSoM; van der Holst et al. 2014) and Gibson-Low flux rope. The two flux ropes differ in orientation and helicity.
- The profiles of magnetic field at Earth are very similar. However, 10 degree ahead of Earth location, the profiles are dramatically different.
- Lugaz et al. (2018) found that the in-situ measurement of CMEs can be quite different in some cases when satellites are separated by 0.01 AU.

To have multiple in-situ measurements around Earth location, we could get a better global picture of magnetic flux rope structure!

Summary

- The first-principles-based MHD global models play an important role in understanding the fundamental physical processes of CME propagation and interaction in the heliosphere. Although still very challenging, it shows promising potential to provide space weather forecast in the near future.
- Data-driven Models: The flux rope is self-consistently formed in the simulation driven by the electric or magnetic fields from observations (e.g., Cheung et al. 2012, Jiang et al. 2016).
- More Observations:
  - Coronal magnetic field/plasma measurements (erupting flux rope structure)
  - L5/polar mission (more coverage of surface magnetic field)
  - Sub-L1 constellation mission (better understanding of magnetic flux rope structure)
- How these “missing data” influence our modeling capability needs to be understand:
  - *How are the modeling of the large-scale magnetic configuration and the resulting solar wind parameters affected by the limited observational coverage of the Sun?*
  - *How do the modeled CME properties depend on the different ambient solar wind and CME flux rope models?*